Macromolecules

Article

pubs.acs.org/Macromolecules

Stochastic Model for Volume Relaxation in Glass Forming Materials: Local Specific Volume Model

Grigori A. Medvedev, Adam B. Starry,† Doraiswamy Ramkrishna, and James M. Caruthers*

School of Chemical Engineering, Purdue University, West Lafayette, Indiana 47907, United States

Supporting Information

ABSTRACT: A stochastic model for structural relaxation in glassy materials is developed, where the rate of relaxation in a mesoscopic domain depends upon the state in that meso-domain. Because the meso-domains have nanometer dimensions, fluctuations are included. The model predicts the volume relaxation for arbitrary thermal histories at ambient pressure in the glass transition region, where the local rate of relaxation is given by a *single* relaxation time that depends on the local density and temperature. Using a single set of parameters, the stochastic model accurately predicts the entire Kovacs poly(vinyl acetate) volume relaxation data set. The meso-domain size was determined to be 2.8 nm, consistent with NMR and other measurements. This model indicates that the origin of the wide relaxation spectra observed experimentally is a single Debye process that experiences significant fluctuations in its state. The stochastic model also naturally predicts the small amount of thermorheological complexity that is observed experimentally near T_g.

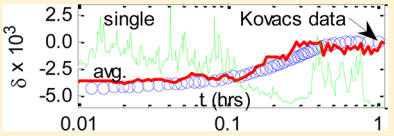

I. INTRODUCTION

One of the most important features of amorphous materials is the liquid-to-glass transition, where a material in a liquid-like state solidifies into a rigid amorphous solid. The formation of the glassy state is observed for a wide range of materials including polymers,[1] small organic molecules,[2] a variety of inorganic materials,[3] and even metals,[4] where almost every material will solidify into the glassy state if the quench rate is sufficiently fast. The liquid-to-glass transition is often characterized by the glass transition temperature, T_g; however, a single temperature cannot even begin to capture the complex, nonlinear dynamics that occur when the glass is formed. This nonlinear relaxation has been observed for a variety of material properties including density, enthalpy, dielectric, and mechanical behavior. Notwithstanding the ubiquitous nature of the glassy state with respect to both the classes of materials and ranges of physical properties that exhibit glassy behavior, a fundamental understanding of the liquid-to-glass transition remains one of the outstanding problems in materials science.[5]

In a classic series of papers,[6,7] Kovacs measured the volume relaxation following a series of single- and two-step temperature jumps for poly(vinyl acetate) (PVAc) in the glass transition region. This is unquestionably the most complete set of volume relaxation measurements for any amorphous material that clearly demonstrates the complexity of the nonlinear relaxation behavior, including non-Debye relaxation, nonlinearity of the initial volume change with respect to the magnitude of the temperature jump, asymmetry in the approach to equilibrium by up vs down temperature jumps of equal magnitude, complex memory behavior for two-step thermal histories, and an expansion gap in the rate of approach to equilibrium for different thermal histories. Although there were small quantitative differences, Kovacs observed similar nonlinear volume relaxation for two different samples of PVAc as well as glucose; moreover, more limited volume relaxation studies on PVAc,[8,9] polystyrene,[10−12] epoxy,[13] and polycarbonate[14] confirm these basic features of the nonlinear volume relaxation, although there is some disagreement over the presence of the expansion gap.[15] In our opinion, the second Kovacs data set[7] for PVAc provides the gold standard for nonlinear volume relaxation exhibited by amorphous materials, and any acceptable theory of relaxation in the liquid-to-glass transition must at a minimum be able to describe this data set.

Numerous structural relaxation models have been proposed to describe time-dependent relaxation behavior in the liquid-to-glass transition region. Although the various models have differences, all these models employ the basic assumption that the rate of volume (or enthalpy) relaxation is proportional to the deviation from equilibrium, where the relaxation time depends upon both the temperature and some parametrization of the nonequilibrium state (i.e., structure) in the glass. Current models for volume relaxation can be divided into three general classes. The *first* class of models, which include the various versions of the KAHR model,[16−19] employ a distribution of relaxation times, where all relaxation times are affected equally by temperature and some nonequilibrium state variable (i.e., the models are thermorheologically simple). The different models assume different functional forms for the distribution of relaxation times and the dependence of the relaxation times on temperature and the nonequilibrium state variable. The *second* class of models assumes a population of relaxation processes that each can relax at a different rate, which include contributions by Robertson[20] and Vleeshouwers and Nies.[21,22] An appealing feature of these models is that the

Received: March 4, 2012
Revised: July 24, 2012
Published: August 31, 2012

   dx.doi.org/10.1021/ma300441a | *Macromolecules* 2012, 45, 7237−7259

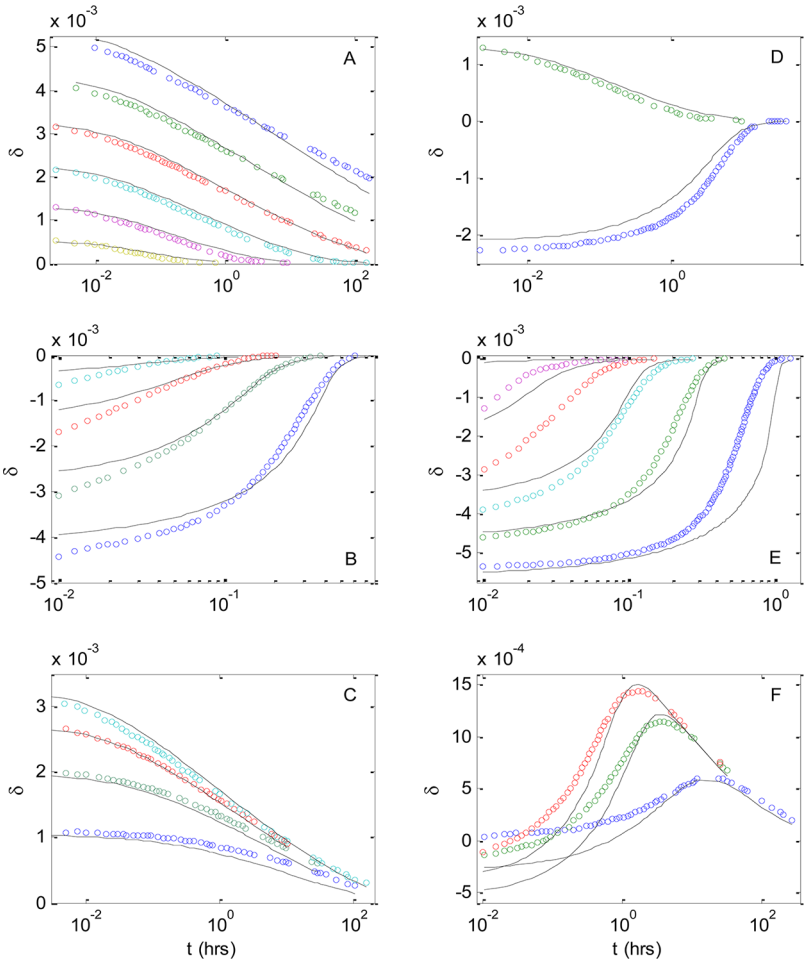

Figure 1. KAHR model prediction of the Kovacs data set. Volume response following: (A) Temperature down-jumps from 40 °C to (in the descending order) 25, 27.5, 30, 32.5, 35, 37.5 °C. (B) Temperature up-jumps to 40 °C from 37.5, 35, 32.5, 30 °C. (C) Temperature down-jumps to 30 °C from 40, 37.5, 35, 32.5 °C. (D) Asymmetry experiment: after temperature down-jump from 40 to 35 °C (upper curve) and after temperature up-jump from 30 to 35 °C (lower curve). (E) Annealing experiment: after temperature down-jump from 40 to 25 °C, annealing for (in the descending order) 0.3, 4, 28, 160, and 1500 h, and temperature up-jump from 25 to 40 °C. (F) Memory experiment: after temperature down-jump from 40 to 10 °C, annealing for 160 h, and temperature up-jump to 30 °C; after temperature down-jump from 40 to 15 °C, annealing for 140 h, and temperature up-jump to 30 °C; after temperature down-jump from 40 to 25 °C, annealing for 90 h, and temperature up-jump to 30 °C. Circles: data; lines: predictions.

relaxation times distribution arises physically from density, or alternatively free volume, fluctuations. In the first two classes of models the rate of relaxation depends upon the instantaneous temperature and state of the material; in contrast, the *third* class of models assumes that relaxation rate is a functional of the thermal and state history and includes contributions by Lustig et al.[23] and Caruthers et al.[24] Models in the third class are thermorheologically simple.

The structural relaxation models listed in the previous paragraph can describe certain features of the experimentally observed volumetric response. However, the predictions from only a limited number of these models have been quantitatively compared to the Kovacs data set;[16−21] moreover, these quantitative comparisons have only been for a fraction of the Kovacs data set. It is not possible in this paper to discuss the predictive capabilities of all the structural relaxation models. However, as a representative example, the predictions for a particular member of the KAHR class of structural relaxation models for the full Kovacs data set are shown in Figure 1, where the KAHR model is formulated as follows: the specific volume departure from its equilibrium (at a given temperature) value

$$\delta = \frac{V - V_0(T)}{V_0(T)} \tag{1}$$

is split into fractions $\{\delta_i\}$ satisfying $\delta = \sum\delta_i$. When the temperature is changing at a rate of q, evolution of each fraction is described as

$$\frac{\mathrm{d}\delta_i}{\mathrm{d}t} = -\frac{\delta_i}{a(T, \delta)\tau_{i,0}} - g_i\Delta\alpha q \tag{2}$$

where the relaxation time distribution is assumed to be of the KWW form[25] and parametrized via a Prony series. Once the values of the KWW parameters β and τ_0 are chosen, the spectrum of the relaxation times (i.e., $\{\tau_{i,0}, g_i\}$ set) is fixed (i.e. thermorheological simplicity). The form of the log a shift function is assumed to be given by[16]

$$\log a(T, \delta) = -\theta_T(T - T_g) - \theta_T(1 - x)\frac{\delta}{\Delta\alpha} \tag{3}$$

The parameter $\Delta\alpha = \alpha_l - \alpha_g = 4.37 \times 10^{-4}$ K^{-1}(i.e., the difference between liquid and glass coefficients of thermal expansion) was determined from the time-independent

dx.doi.org/10.1021/ma300441a | *Macromolecules* 2012, 45, 7237−7259

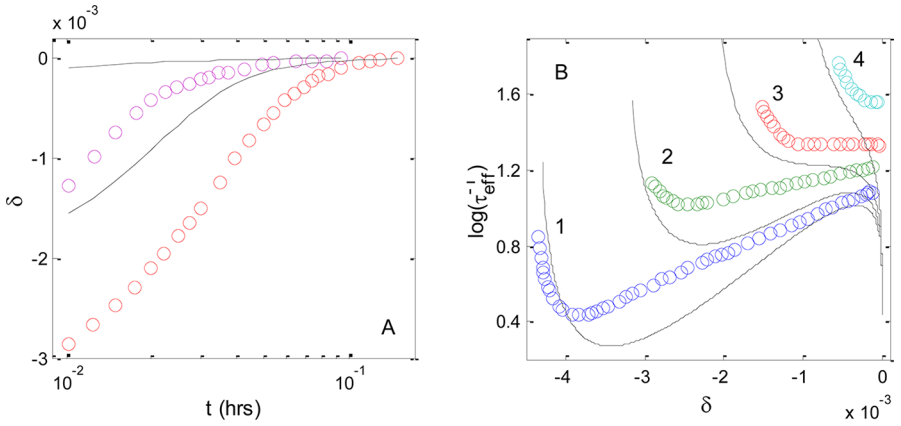

Figure 2. KAHR model difficulties in predicting: (A) Volume response after the "short anneal": temperature down-jump from 40 to 25 °C, annealing for 0.3 h (upper curve) or 4 h (lower curve), and temperature up-jump from 25 to 40 °C. (B) "Expansion gap": τ-effective response after the temperature up-jump from (1) 30, (2) 32.5, (3) 35, and (4) 37.5 °C to 40 °C. Circles: data; lines: predictions.

volume−temperature data.[26] The remaining model parameters were determined by optimization with respect to the Kovacs[7] data set comprised of 23 distinct thermal histories, where the optimum parameters are $\tau_0 = 5.79 \times 10^4$ s, $\beta = 0.44$, $x = 0.215$, and $\theta_T = 0.85$ K^{-1}. The predictions shown in Figure 1 are good for most of the data set; however, the KAHR model does have some difficulties. Specifically, the well-known τ-effective (i.e., $\tau_{\text{eff}} = \delta^{-1}\, d\delta/dt$) plot for up-jumps to 40 °C is shown in Figure 2B, where there is a significant disagreement between the prediction of the model and the experimentally measured expansion gap. A thorough investigation by Ng and Aklonis[27] showed that KAHR type models are incapable of reproducing the expansion gap, even at the expense of the rest of the Kovacs data set. The inability of KAHR models to describe the expansion gap led some researchers to questioning the validity of the Kovacs data.[28] However, McKenna et al.[15] in a statistical analysis of the original Kovacs data have shown that the expansion gap data are valid with the implication that there is a deficiency in the KAHR model.

A second difficulty in the KAHR class of models is a marked discrepancy between the data and theory for the short annealing time experiments shown in Figure 2A. This difficulty is particularly troublesome, since these should be relatively easy experiments to predict because the amount of relaxation is small. Similar to the expansion gap, the short annealing time predictions of KHAR cannot be improved even by sacrificing the fit to the rest of the data. In summary, the KAHR model, or its close relatives, can describe a number of the features of the Kovacs data set well but is unable to predict other important features of the data. Since a model for structural relaxation should be able to describe the entire Kovacs data, something is missing in the KAHR model for structural relaxation—a fact that is appreciated by most practitioners in this field.

Robertson et al.[20] have proposed a structural relaxation model, where the source of the relaxation times distribution is density fluctuations; however, the predictions of this model when compared to the entire Kovacs data are less than satisfactory. In particular, neither the original Robertson et al.[20] nor a modification by Vleeshouwers and Nies[21] can describe a set of simple down-jump experiments (see Figure 2 in ref 21). Since the discrepancies in the down-jump predictions are so large, there is no hope of reproducing multiple temperature step experiments. Subsequently, Robertson et al.[29] attempted to alleviate this problems by the introduction of two different expressions for the log a function—one above and one below a critical temperature—but even these two log a functions could not produce a fit to the entire Kovacs data set. In the Robertson et al.[20] model log a was assumed to depend upon the fractional free volume via the Doolittle equation,[30] where the fractional free volume was determined from the Simha−Somcynsky equation of state.[20] Alternatively, Vleeshouwers and Nies[21] used the Holey−Huggins model instead of the Simha−Somcynsky model. There are, however, other alternatives to the Doolittle/Simha−Somcynsky or Doolittle/Holey−Huggins log a models.

In this report we will explore the volume based log a models used in conjunction with a stochastic volume relaxation model. The stochastic model can be cast into a master equation form that is similar to that employed by Robertson et al.[20] We will show that by employing a log a with the appropriate volume−temperature dependence in conjunction with a rigorous implementation of the stochastic model nearly all features of the Kovacs data set can be accurately described with only a *single* relaxation time. This is a significant simplification compared to the spectrum of relaxation times used in the traditional viscoelastic models of structural relaxation. However, this simple stochastic model is unable to predict the pressure dependence of T_g, where this difficulty will be addressed in a future publication that incorporates fluctuations in both the volume and configurational entropy.

The remainder of this paper is organized as follows: in section II, the stochastic model will be developed in three equivalent forms: stochastic differential equation (SDE), Fokker−Planck equation (FPE), and master equation (ME). Also the form of the temperature and volume dependence of log a will be developed. In section III we will describe how the model parameters were determined by optimization to the Kovacs PVAc volume relaxation data and compare the predictions of the model to the data. Finally, we will critically discuss the capabilities, implications, and needed improvements of the stochastic model. Since the primary audience of this paper is researchers interested in polymeric and other glass-forming materials, the paper will focus on the physical formulation of the model, its predictions, and the physical implications of those predictions. The formulation involves a nonlinear SDE and the associated nonlinear FPE and ME mathematical methods that are typically unfamiliar to most polymer glass researchers; consequently, the detailed mathe-

dx.doi.org/10.1021/ma300441a | *Macromolecules* 2012, 45, 7237−7259

matics used in the theoretical development have to the extent possible been relegated to the Appendices in order to minimize disturbance to the flow of the physical ideas.

II. THEORY

Motivation for Development of the Stochastic Model. We postulate that a model for structural relaxation that employs only macroscopic parameters will be an incomplete description of the glass transition region, since it does not acknowledge the inherently heterogeneous nature of the glassy state. Considerable experimental evidence clearly indicates that motional heterogeneity does exist in glass forming materials in the vicinity of the glass transition (e.g., see the reviews by Sillescu,[31] Ediger,[32] and Berthier[33] and the extensive references therein). Specifically, in the glassy state and glass transition region, chemically homogeneous molecular glass-formers and segments of the same chemical structure in polymers reorient at vastly different rates, depending upon their physical location in space; thus, the molecular dynamics near T_g is heterogeneous for time scales much longer than the average motional correlation time. This large distribution of motional dynamics has been experimentally observed using multidimensional NMR in several different glass-forming polymeric materials including PVAc,[34−36] polystyrene,[37] and polycarbonate.[38] The existence of motional heterogeneity is also supported by anomalous light scattering of inorganic glass formers like B_2O_3[39] and heavy metal fluoride glasses.[40−42] By assuming that these heterogeneities give rise to the distribution of relaxation times, Moynihan and Schroeder[41] estimated the size of the density heterogeneities for B_2O_3, glycerol, and PVAc between 2.3 and 4.6 nm at their respective glass transition temperatures. Further evidence for the presence of dynamic heterogeneities is furnished by the dielectric hole burning[43] and the solvation dynamics[44] experiments. In addition to this direct experimental evidence, there are a number of other arguments that support the idea of dynamic heterogeneity. First, the nonexponential relaxation has usually been interpreted as arising from a distribution of correlation times, where various researchers have postulated that the amorphous material consists of spatially separated regions of relatively high and low mobility that maintain their identity for times longer than the largest correlation time (see review[32] by Ediger). Of course, a non-single-exponential relaxation response is not by itself a unique indication of spatial heterogeneity, since a spatially homogeneous, non-Debye process is also a possibility. Second, the breakdown of Stokes−Einstein−Debye relationship in the vicinity of glass transition can be explained via dynamic heterogeneities.[45,46] Third, using the AFM technique, Russell et al.[47,48] observed nanoscale dielectric fluctuations in PVAc near glass transition. Finally, the heterogeneous nature of the glassy state has been observed in molecular dynamic simulations.[49−51]

An inescapable conclusion of acknowledging spatial heterogeneity is that an appropriate description of structural relaxation should be sought on the level of the mesoscopic domains rather than the macroscopic sample as a whole. The development of a model that explicitly acknowledges mobility heterogeneity is the objective of this communication. A model of spatially distributed and interacting domains should be formulated in terms of a continuous spatial description of the relevant field variables; however, a full field description is intractable by current field theoretical methods. Thus, in order to avoid a full spatial description, we postulate that the glass forming material can be spatially coarse grained into domains of characteristic length L each with a different mobility. We will also assume (i) all information about the state of a domain is adequately represented by spatially uniform domain properties (i.e., all gradients are neglected) and (ii) the interaction between domains is approximated via a mean field. A key model assumption will be how the variable that controls the mobility in a representative domain depends upon the combination of local and mean field values of that variable. Robertson[20] proposed that in a free volume model of the local shift factor, log a, was not a function of just the local specific volume, v, but rather was the same Dolittle function of the quantity

$$\frac{1}{z}v + \frac{z-1}{z}V \tag{4}$$

where V is the macroscopic (i.e., average) specific volume and z is an interaction parameter. Clearly, $z = 1$ corresponds to the case of noninteracting domains, and $z = \infty$ corresponds to the macroscopic limit. Compared to the traditional models, the mesoscopic description introduces two new parameters: L, which is a characteristic size of the domain (i.e., the length scale of spatial coarse-graining of the system), and z, which describes the cooperativity between the meso-domains. The size of a domain controls the magnitude of the fluctuations of thermodynamic properties and, as will be shown, parametrizes the width of the associated relaxation response. The parameter z can be considered a coordination number of the local domains that must tile space.

Formulation of the Defining Stochastic Differential Equation (SDE). We will first focus on the dynamic behavior of an individual domain. In this paper it will be assumed that volume is the only variable that affects the dynamic response, where the temperature and pressure are externally controlled parameters. There are other alternatives for the mobility relationship, including configurational entropy,[52] configuration internal energy,[24] and stress.[53] If configurational entropy controls mobility, a description of the dynamics will require the simultaneous description of volume and configurational entropy, which we will develop in a subsequent paper. In the present paper we will describe the response using the simple assumption of just one fluctuating variable: the specific volume. The description of a fluctuating system can be obtained in terms of either (i) a stochastic differential equation (SDE) which describes the time evolution of a single realization of the dynamic system, (ii) a Fokker−Planck equation (FPE) which describes the temporal evolution of the probability distribution of the dynamic variable, or (iii) a master equation (ME) which describes the evolution of a discretized probability density. These three descriptions are formally equivalent but provide different perspectives of the relaxation process. The SDE formulation is the most physically transparent and provides a description of what occurs in a specific meso-domain. The FPE provides the most appropriate description of the average response, and the ME often is the most efficient method for numerical solution. We will exploit the features of all three methods, starting with the SDE formulation of the physical problem.

The key postulate in the stochastic model of the glassy response is that the local (i.e., mesoscopic) relaxation time is explicitly related to the local state variable. It seems natural to start with a traditional relaxation equation used for a macroscopic system and then generalize the macroscopic description to take into account the fluctuations that cannot be

neglected on the mesoscopic level. The simplest model for volume relaxation is given by[6]

$$\frac{\mathrm{d}V}{\mathrm{d}t} = -\frac{V - V_\mathrm{e}}{a(V, T)\tau_0} + V\alpha_\mathrm{g}\frac{\mathrm{d}T}{\mathrm{d}t} - V\beta_\mathrm{g}\frac{\mathrm{d}P}{\mathrm{d}t} \tag{5}$$

where $a(V,T)$ is the shift function, τ_0 is the relaxation time in a reference state, α_g is the glassy coefficient of thermal expansion, and β_g is the glassy compressibility. This single relaxation time equation assumes that the rate of approach to equilibrium is proportional to the deviation from equilibrium, where the "constant" of proportionality is a function of the current state of the system (i.e., temperature and volume in the current paper). The key idea is to replace the standard relaxation equation by an SDE that accounts for mesoscopic fluctuations. A possible way of building the defining SDE would be replacing the macroscopic specific volume V with the local specific volume v and augmenting the macroscopic relaxation equation with a noise term; consequently, the isothermal−isobaric form of eq 5 including fluctuations is

$$\mathrm{d}v = -\frac{v - V_\mathrm{e}}{a(v, T)\tau_0}\,\mathrm{d}t + N(v, T)\,\mathrm{d}W \tag{6}$$

Equation 6 describes evolution of local volume v and includes a "drift" term coinciding with the deterministic equation given in eq 5 and a "noise" term assumed to be a Wiener process $W(t)$ of magnitude $N(v,T)$. The magnitude of the noise is not arbitrary, but rather it is dictated by the requirement that the stationary volume distribution be consistent with equilibrium thermodynamics. The distribution of the specific volume resulting from the solution of the SDE must, in the limit of large times, approach the Gaussian function required by equilibrium thermodynamics, specifically

$$p^{(s)}(v) = \frac{1}{\sqrt{2\pi}\sigma_\mathrm{e}}\exp\left[-\frac{(v - V_\mathrm{e})^2}{2\sigma_\mathrm{e}^2}\right] \qquad \sigma_\mathrm{e}^2 = \frac{1}{L^3}V_\mathrm{e}^2 k_\mathrm{B}T\beta_\mathrm{e} \tag{7}$$

$p^{(s)}(v)$ is the stationary probability distribution of v, and $V_\mathrm{e}(T)$ is the equilibrium volume. $\sigma_\mathrm{e}(T)$ is the width of the distribution, which is a function of the domain size L, the isothermal compressibility $\beta(T)$, and the Boltzmann constant k_B.

Although eq 6 is the straightforward generalization of the isothermal−isobaric form of eq 5, the form of eq 6 is such that the required stationarity can only be achieved if $a(v,T)$ is a constant—an uninteresting case, since volume dependence of $a(v,T)$ is the dominant nonlinearity. The problem is that when the $a(v,T)$ shift factor is a function of v, the drift term in eq 6 is so asymmetric that no form of the noise term $N(v,T)$ can compensate so that a stationary distribution as required by eq 7 will occur. In Appendix A we show that in order to satisfy stationarity, eq 6 has to be replaced by a more general SDE of the form

$$\mathrm{d}v = A(v, T)\,\mathrm{d}t + \sigma_\mathrm{e}B(v, T)\,\mathrm{d}W \tag{8}$$

where the drift term $A(v,T)$ is *not* the simple relaxation term $-(v - V_\mathrm{e})/a(v,T)\tau_0$. There are two choices for the functions $A(v,T)$ and $B(v,T)$ that satisfy stationarity (see Appendix A):

Case I:

$$A = \sigma_\mathrm{e}^2\frac{\mathrm{d}R}{\mathrm{d}v} - (v - V_\mathrm{e})R \tag{9a}$$

$$B^2 = 2R \tag{9b}$$

Case II:

$$A = \sigma_\mathrm{e}^2\left\langle\frac{\mathrm{d}R}{\mathrm{d}v}\right\rangle_\mathrm{e} - (v - V_\mathrm{e})R \tag{10a}$$

$$B^2 = 2R + \frac{2}{p^{(s)}}\left[\left\langle\frac{\mathrm{d}R}{\mathrm{d}v}\right\rangle_\mathrm{e}\int_{-\infty}^{v} p^{(s)}\,\mathrm{d}v' - \int_{-\infty}^{v}\frac{\mathrm{d}R}{\mathrm{d}v'}p^{(s)}\,\mathrm{d}v'\right] \tag{10b}$$

where $R = 1/a(v,T)\tau_0$ is the instantaneous relaxation rate and $\langle\,\rangle_\mathrm{e}$ denotes averaging with the stationary (i.e., equilibrium) distribution $p^{(s)}(v)$ given in eq 7. Depending on the functional form of $a(v,T)$, the difference in the time-dependent behavior predicted by these two cases can be significant. We are not aware of any physical reason that would indicate *a priori* whether case I or case II is the appropriate stochastic generalization; however, as will be discussed below, we were unable to find a set of parameters that result in a reasonable fit to the Kovacs data set for case II. Thus, eqs 8 and 9 are the appropriate stochastic generalization of the standard deterministic relaxation equation given in eq 5.

Formulation of the Fokker−Planck Equation (FPE) and Master Equation (ME). The SDE formulation given by eqs 8 and 9 is a complete statement of the proposed model, where a particular realization of eqs 8 and 9 describes an instance of the evolution of a given mesoscopic domain in the sample. The macroscopic response is determined by averaging over an ensemble of individual realizations. However, the solution of the SDE is computationally intense, since a vanishingly small time step is required when a domain experiences a large positive volume fluctuation that causes the relaxation rate to be very fast; thus, numerically averaging the SDEs for the full Kovacs data set is computationally inefficient. The FPE is a deterministic equation for the evolution of the probability, avoiding the need for the ensemble average. The FPE corresponding to the SDE defined in eq 8 is given by[54]

$$\frac{\partial}{\partial t}p = -\frac{\partial}{\partial v}(Ap) + \frac{\sigma_\mathrm{e}^2}{2}\frac{\partial^2}{\partial v^2}(B^2 p) \tag{11}$$

where $p = p(v,t)$ is the normalized, nonequilibrium probability density of the specific volume v. Whereas the SDE was an ordinary differential equation in time, the FPE is a partial differential equation in time and specific volume; thus, the FPE is more difficult to solve, but there is no need for computing the ensemble average. For mathematical convenience the variable v is considered on an infinite domain (i.e., $v \in [-\infty, \infty]$), where the $p(v,t)$ must vanish when v is significantly different from the macroscopic average specific volume V and must be zero for any v less than the hard core specific volume. The probability density at $t = 0$ is the initial condition for the FPE.

If the volume space is discretized into n states (i.e., $v = \{v_i\}$), the local volume distribution $\{p_i\}$ can be equivalently described by a birth−death master equation (ME) of the form[54]

$$\frac{\partial}{\partial t}p_i = k_{i-1}^{+}p_{i-1} + k_{i+1}^{-}p_{i+1} - (k_i^{+} + k_i^{-})p_i \qquad i = 1, \ldots, n \tag{12}$$

with the reflecting boundary conditions

$$k_1^{-} = 0, \quad k_n^{+} = 0, \quad p_0 = 0, \quad p_{n+1} = 0 \tag{13}$$

dx.doi.org/10.1021/ma300441a | Macromolecules 2012, 45, 7237−7259

where k_i^+ is the transition rate from the i to the $i + 1$ state and k_i^- is the transition rate from the i to the $i - 1$ state. The reflecting boundary conditions force the probability distribution to remain confined within the volume discretization interval from $i = 1$ to n. The FPE given in eq 11 and the ME given in eq 12 are equivalent, when the upward and downward rates are[54]

$$k_i^- = -\frac{A(v_i)}{2h} + \frac{\sigma_e^2 B^2(v_i)}{2h^2} \quad k_i^+ = \frac{A(v_i)}{2h} + \frac{\sigma_e^2 B^2(v_i)}{2h^2} \tag{14}$$

where h is the step between two consecutive values of discrete variable v_i. It can be shown that the solution of eq 12 approaches that of the original FPE as the size of the discretization h goes to zero. The discretized stationary distribution $p_i^{(s)}$ satisfies the detailed balance relations

$$k_{i-1}^+ p_{i-1}^{(s)} = k_i^- p_i^{(s)} \tag{15}$$

It is interesting that the transformation to the ME form seems to suggest that the case I is more natural as is discussed in Appendix B.

The FPE and ME provide formally equivalent descriptions to the SDE. The FPE was necessary to determine the functional forms of $A(v,T)$ and $B(v,T)$. The ME formulation is computationally more efficient. Finally, the SDE is the physically most transparent formulation of the problem and, thus, provides a picture of the behavior of a single mesoscopic domain (see Discussion) and a better starting point for generalization of the model; however, determination of the macroscopic response is computationally expensive using the SDE formulation.

Mesoscopic Model of the $a(v,T)$ Shift Function. So far the derivation of the stochastic model has been independent of the form of the log $a(v,T)$ shift function, but now the exact functional form must be specified. The form of the mesoscopic log $a(v,T)$ is more important in the mesoscopic model developed in this communication than in macroscopic volume relaxation models, because a mesoscopic domain samples much larger region in the temperature−volume space than the macroscopic system. Direct experimental measurements of the mesoscopic log $a(v,T)$ function are not available. Thus, we will not attempt to divine the "true" expression for log $a(v,T)$; rather, we will postulate a simple form for mesoscopic log $a(v,T)$ with an adjustable parameter and then determine if using this simple form for log $a(v,T)$ the stochastic model can predict the volume relaxation for the Kovacs data set.

A key concept is the difference between the macroscopic log a and the mesoscopic log a. Macroscopic log a in the glass depends upon the thermal/deformation path used to create the glass and thus is a functional[24] of the temperature/deformation history. However, it has been shown[16,55] that for a limited range of conditions one can describe certain macroscopic responses with a log a that is a function of volume and temperature, even though in general a functional description is needed. The mesoscopic log a is fundamentally different, where locally large volume fluctuations will erase any knowledge of the macroscopic volume history (see the local volume response vs the macroscopic volume response shown in Figure 10 in the Results section). Thus, the mesoscopic log $a(v,T)$ function is most appropriate vs a log a functional of the volume and temperature histories that is needed for a macroscopic description—the question is to determine the temperature and volume dependence of the mesoscopic log $a(v,T)$. Although for nonlinear, stochastic equations there is no assurance that the ensemble average of a quantity will have the same functional form as the related term in the SDE, we will assume that macroscopic forms proposed for log $a(v,T)$ can provide guidance for determining the mesoscopic log $a(v,T)$ needed in the current stochastic model for volume relaxation.

One postulate for the macroscopic equilibrium log a is the pressure modified WLF equation (see review by Tschogel et al.[56] and references therein)

$$\log a = -c_1 + c_1 \frac{c_2}{c_2 + T - T_g(P)} \quad T_g(P) = T_g + \gamma P \tag{16}$$

where T_g is the glass transition at $P = 0$ and the parameter $\gamma = dT_g/dP$ is the slope of the glass formation line. If it is assumed that the PVT surface is a plane, the log $a(V,T)$ expression for an equilibrium material is given by

$$\log a(V, T) = -c_1 + c_1 \frac{c_2}{c_2 + T - T_g + \frac{\gamma}{V_g \beta_l}[V - V_0(T)]} \tag{17}$$

where β_l is the isothermal liquid compressibility, $V(T,P=0) \equiv V_0(T) = V_g[1 + \alpha_l(T - T_g)]$, α_l is the liquid thermal expansion coefficient, and V_g is the specific volume at T_g. It is informative to look at the isomobility lines in VT-space which for the log a model given in eq 17 are given by

$$\left.\frac{dV}{dT}\right|_{\log a} = -\frac{V_g \beta_l}{\gamma} + V_g \alpha_l \tag{18}$$

In the nonequilibrium glassy state at $P = 1$ atm, it is typically assumed that the essential features of the mobility will be captured if log a is made a function of the current nonequilibrium volume. The standard approach is to substitute the temperature in an equilibrium expression for log a by the fictive temperature, T_f, which depends on volume according to[55]

$$T_f = T + \frac{V - V_0(T)}{V_g} \frac{1}{\alpha_l - \alpha_g} \tag{19}$$

If the equilibrium log a expression is assumed to be Arrhenian, then replacement of T with $xT + (1 - x)T_f$ results in the Narayanaswamy log a model,[57] which has been used extensively in conjunction with the KAHR formalism.[16] On the other hand, if the equilibrium behavior is described by the WLF function, the substitution of the fictive temperature results in the expression

$$\log a(V, T) = -c_1 + c_1 \frac{c_2}{c_2 + T - T_g + \frac{V - V_0(T)}{V_g(\alpha_l - \alpha_g)}} \tag{20}$$

The isomobility lines for the log $a(V,T)$ model given in eq 20 are

$$\left.\frac{dV}{dT}\right|_{\log a} = V_g \alpha_g \tag{21}$$

The mesoscopic log $a(v,T)$ needs to describe both the behavior in the equilibrium state, where eq 17 is most appropriate, as well as in the glassy state, where eq 20 is most appropriate. Perhaps in macroscopic volume relaxation models one can use a different log a expression when in the equilibrium vs the glassy state; however, in a mesoscopic model where the

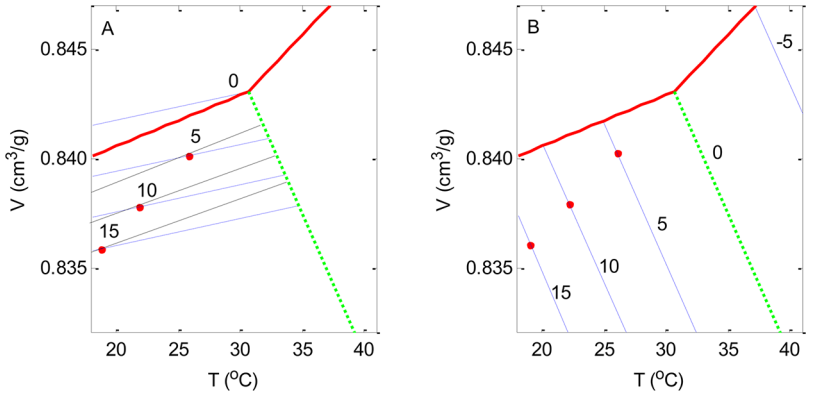

Figure 3. Isomobility lines (i.e., log a = const in V–T space. Heavy solid line: experimental V vs T at 1 atm for PVAc;[26] dotted line: glass formation line[26] ($V_g(P)$, $T_g(P)$); numbers indicate the log a values; filled circles: points along the equilibrium line $V = V_e(T,P = 1$ atm). (A) log a from fictive temperature model in eq 20: light solid lines; log a from eq 22 with s optimized to fit the Kovacs data (see Table 1): blue lines; (B) equilibrium state log a from eq 17: blue lines.

material is undergoing large fluctuations, the log $a(\nu,T)$ function must be able to capture the mobility in both the equilibrium and glassy states. This may not be possible to achieve with a log a model that only depends upon temperature and volume, but these are the only variables that are available in the current framework. The log $a(V,T)$ models given in eqs 17 and 20 were developed as descriptions of the *macro*scopic mobility, with the caveat that eq 17 is used for an equilibrium material and eq 20 is an empirical expression that has been used to describe mobility for a glassy material at 1 atm. However, a *meso*scopic log $a(V,T)$ model needs to have features of both expressions, since the local material will fluctuate between the glassy and liquid state. In order to interpolate between eqs 17 and 20, the slope $s = [\mathrm{d}V/\mathrm{d}T]_{\log a}$ will be a model parameter, and the expression for log $a(V,T)$ is

$$\log a(V, T) = -c_1 + c_1 \frac{c_2}{c_2 + T - T_g + \frac{V - V_0(T)}{V_g\alpha_l - s}} \tag{22}$$

The parameter s will be determined from optimization over the Kovacs data set. Changing s causes the isomobility lines to rotate about the ($T = T_g$, $V = V_g$) point. For PVAc, eq 20 is recovered when $s = V_g\alpha_g = 2.345 \times 10^{-4}$ g/(cm^3 K) and eq 17 is recovered when $s = V_g(\alpha_l - \beta_l/\gamma) = -16.2 \times 10^{-4}$ g/(cm^3 K). An alternative derivation of eq 22 would be to replace T in the WLF equation with $xT + (1 - x)T_f$ where the parameter x is related to the slope s as $s = V_g(\alpha_g - x\alpha_l)/(1 - x)$.

The isomobility lines for the two log $a(\nu,T)$ expressions—eq 22 with the value of s optimized to fit Kovacs data and eq 17—are shown in Figure 3. log a is the same for both models along the $P = 1$ atm line for an equilibrium material; however, away from equilibrium the two log $a(\nu,T)$ are quite different. The isomobility lines for the fictive temperature-based log a model have a slope that is similar to the slope of the glassy specific volume; however, this model is qualitatively unable to describe the formation pressure dependence of T_g. In contrast, the log a model given in eq 17 is constructed so that $T_g(P)$ is captured, but this log a model has not been successfully in describing volume relaxation data for KAHR and similar types of macroscopic volume relaxation models.

Finally, an expression for the local log a is obtained from eq 22 by replacing the macroscopic volume with the combination of the local and average volume given in eq 4, giving rise to

$$\log a(\nu, T) = -c_1 + c_1 \frac{c_2}{c_2 + T - T_g + \frac{\frac{1}{z}\nu + \frac{z-1}{z}V - V_0(T)}{V_g\alpha_l - s}} \tag{23}$$

This is the simplest form for log $a(\nu,T)$ that preserves the WLF equation along the atmospheric pressure line and results in linear isomobility lines in VT-space. We acknowledge that other forms of log a could also be used and if an alternative expression for log $a(\nu,T)$ becomes available, the incorporation into the stochastic formalism is straightforward.

Solution of the Master Equation. The solution of the ME with the log $a(\nu,T)$ function given by eq 23 is obtained using standard eigenvector methods as detailed in Appendix C. Because of the wide range of relaxation times in the glass, a perturbation solution was used for evaluation of the eigenvalues and eigenvectors as detailed in the Supporting Information. Of particular concern is the level of discretization needed for $\nu = \{\nu_i\}$. Numerical studies described in Appendix C show that if $n > 150$, the discrete solution of the ME is equivalent to the continuous FPE for the thermal histories contained in the Kovacs data set. The solution procedure for an arbitrary temperature history is the following:

1. Every temperature ramp is divided into intervals of the size ΔT such that the time required for the temperature to change by ΔT is $\Delta t = \Delta T/|q|$ seconds, where q is the externally controlled cooling/heating rate.

2. The continuous change in temperature is approximated for a given interval, say from T to $T - \Delta T$, as a two-stage process: temperature instantly reaches its final value and then remains constant for the rest of the time period of Δt.

3. The instantaneous change in temperature is accompanied by the instantaneous change in the specific volume, which constitutes the elastic part of the response. The magnitude of the elastic change is given by $\Delta V = \alpha_g V_g \Delta T$. Since no relaxation can occur during the instantaneous temperature jump, the entire distribution of local specific volumes shifts uniformly by ΔV; i.e., there is no change in the shape of the distribution.

4. Isothermal relaxation toward the new equilibrium distribution at $T - \Delta T$ (i.e., $p^{(s)}(T - \Delta T)$) proceeds for Δt seconds.

The solution algorithm for the isothermal response based on the ME formulation is described in Appendix C. A pressure history can be treated in an analogous fashion.

dx.doi.org/10.1021/ma300441a | *Macromolecules* 2012, 45, 7237–7259

The above procedure introduces an error that increases with the size of the discretization step ΔT, especially at higher temperatures. Since changes in temperature always occur over a finite time, the domains with higher mobility (i.e., those domains with the higher value of current volume) may be able to keep up with the pace of cooling/heating whereas the domains of lower mobility may not, thus violating the assumption that the volume distribution shifts uniformly during the temperature jump. For example, using the PVAc parameters determined from fitting the Kovacs data set (see next section), in the equilibrium state at 40 °C the relaxation time for a domain with the specific volume exceeding the average by $3\sigma_e$ is ~0.4 s; in contrast, the relaxation time for a domain with the specific volume that is smaller than the average by $3\sigma_e$ is $\sim 6 \times 10^3$ s. For temperatures of 40 °C or less, making the temperature step ΔT less than 0.25 °C causes no further changes in the volume relaxation results, where the results between ΔT = 0.25 °C and ΔT = 1.0 °C differ by less than 1%. The value of ΔT = 0.25 °C is used to obtain all the results reported in this paper.

III. RESULTS

Predictions of the Stochastic Model for the Kovacs Data Set. *Determination of Model Parameters.* The material parameters for the stochastic model are given in Table 1. The

Table 1. Parameters of the Stochastic Model

T_g	c_1	c_2	τ_0	z	L	s
31 °C	16.8	42.56 °C	7.18 h	6.9	2.84 nm	1.22×10^{-4} g/(cm^3 K)

WLF parameters c_1 and c_2 are set by fitting the log a vs temperature data for an equilibrium material at 1 atm. A variety of isobaric data are available for PVAc, including dielectric relaxation,[58−63] mechanical relaxation,[61,64−71] and the DSC.[61,72,73] The various data were shifted such that log a = 0 at a unified reference temperature of T_g = 31 °C and are shown in Figure 4, where the WLF constants are c_1 = 16.8, c_2 = 42.56 °C.

These WLF parameters only slightly differ from the ones reported by Ferry[74] and used by Robertson et al.,[20] where c_1' = 17.06, c_2' = 42.8 °C (these were determined by shifting the reported values of c_1 and c_2 to 31 °C). Later Robertson et al.[29] and Vleeshouwers and Nies[21] used a significantly different parameter set of c_1'' = 14.88, c_2'' = 24.74 °C determined by Plazek[75] from torsional creep recovery. The ratio 2.303 c_1/c_2 equals the θ_T parameter of the linearized KAHR model, where Greener et al.[16] reported θ_T = 0.85 K^{-1} for the Kovacs PVAc data and the Plazek data set gives rise to 2.303 c_1''/c_2'' = 1.385 K^{-1}. Our objective is not to resolve these differences, but to show that the WLF parameters used here agree with the majority of the literature data as shown in Figure 4.

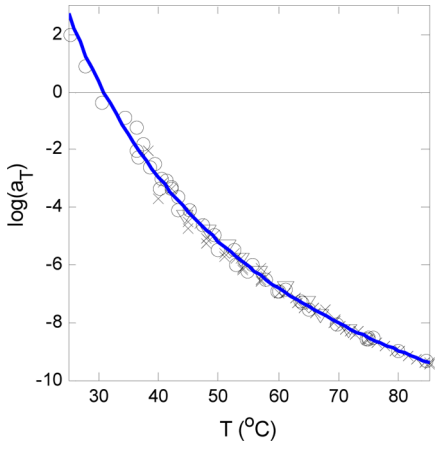

Figure 4. PVAc shift factor at atmospheric pressure from relaxation data (see text for references): circles, mechanical; crosses, dielectric; triangles, enthalpy. Solid line: WLF fit.

The remaining four parameters in the stochastic model are (i) the slope s of the isomobility lines, (ii) the domain size L, (iii) the cooperativity z, and (iv) the reference time τ_0. For numerical solution the FPE, i.e., eqs 11 and 23, have been put into dimensionless form (see Supporting Information for details), where the coefficient of the dimensionless volume v/σ_e is σ_e/z plus a weak contribution from σ_e alone (i.e., as a coefficient in front of V/σ_e). Since σ_e is a function of L via eq 7, the parameters z and L are strongly correlated. If the effects of the tails of the distribution are small, the $\{z, L\}$ set is effectively a single model parameter. The predictions for any thermal history from the Kovacs data set change by less than 10% for z = 3 to z = 15 provided the values of L are adjusted to keep σ_e/z constant. The stochastic model has four adjustable parameters: s, τ_0, and $\{z, L\}$, the latter two being strongly correlated—which will be determined from optimization to the Kovacs volume relaxation data.

The solution of the stochastic model requires the detailed thermal history. However, the only information for the Kovacs experiments was that thermal equilibration was completed within less than 36 s.[7] Consequently, we have assumed that all the temperature changes occurred at a constant rate of $|q|$ =1 °C/s. Because the details of the thermal history become increasingly important at higher temperatures, Kovacs thermal histories where temperature at any point exceeded 40 °C have been excluded from the optimization set. The case I alternative of stochastic model was optimized over all thermal histories in the Kovacs data set[7] (except for data above 40 °C) using the *fminsearch* function in MatLab that employs a simplex algorithm. The objective function for optimization was constructed as follows: Sum of squared differences between experimental values and predictions was calculated for each curve in Figure 5. Then for each curve the result was divided by the number of data points in it to prevent the objective function from being dominated by the experiments with the largest number of points. Finally, in order to more effectively fit curves that exhibit only small deviations from equilibrium, the contributions from the curves for which for all points $|\delta| < 1.5 \times 10^{-3}$ were multiplied by 5 (this includes, for example, memory experiments).

Stochastic Model Predictions of the Kovacs Data Set. The results for best fit of the case I stochastic model are shown in Figure 5 with the optimized parameter values given in Table 1. The stochastic model does an excellent job of fitting the whole Kovacs data set. Comparing the Stochastic and KAHR models, the stochastic model does a better job of fitting the (i) up-jump data in Figures 1B/5B, (ii) the 25 °C annealing data in Figures 1E/5E, and the (iii) memory experiment in Figures 1F/5F. The KAHR model does a slightly better job of describing (i) the down-jump data from 40 °C in Figures 1A/5A and (ii) down-jump data from 30 °C in Figures 1C/5C. The memory experiment in Figures 1D/5D was described with nearly equal precision by both models. Based upon overall quality of fit,

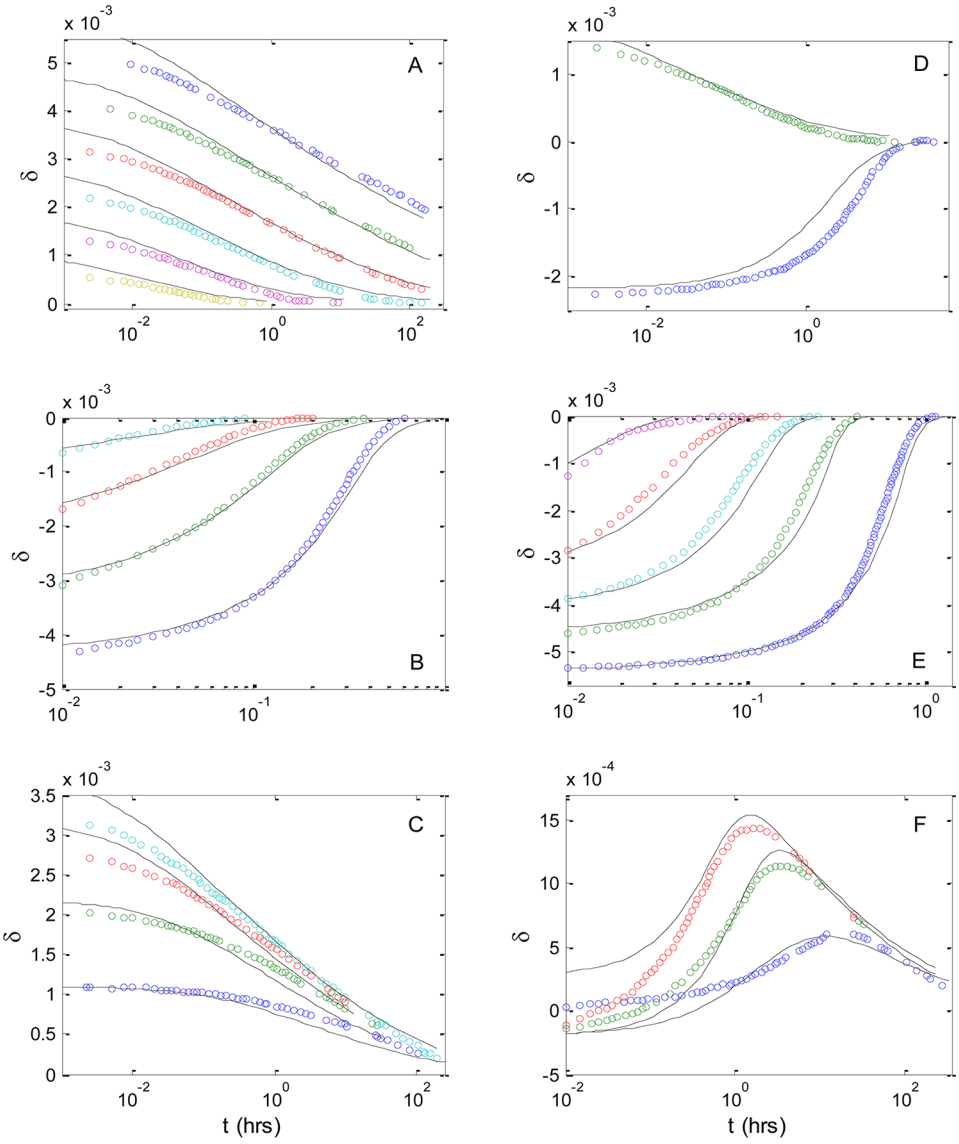

Figure 5. Stochastic model prediction of the Kovacs data set. Volume response following: (A) Temperature down-jumps from 40 °C to (in the descending order) 25, 27.5, 30, 32.5, 35, 37.5 °C. (B) Temperature up-jumps to 40 °C from 37.5, 35, 32.5, 30 °C. (C) Temperature down-jumps to 30 °C from 40, 37.5, 35, 32.5 °C. Circles: data; lines: predictions. (D) Asymmetry experiment: after temperature down-jump from 40 to 35 °C (upper curve) and after temperature-up jump from 30 to 35 °C (lower curve). (E) Annealing experiment: after temperature down-jump from 40 to 25 °C, annealing for (in the descending order) 0.3, 4, 28,160, 1500 h and temperature up-jump from 25 to 40 °C. (F) Memory experiment: after temperature down-jump from 40 to 10 °C, annealing for 160 h, and temperature up-jump to 30 °C; after temperature down-jump from 40 to 15 °C, annealing for 140 h, and temperature up-jump to 30 °C; after temperature down-jump from 40 to 25 °C, annealing for 90 h, and temperature up-jump to 30 °C. Circles: data; lines: predictions.

there is little difference between the two models; however, there are significant differences in the details of the predictions which will be subsequently discussed.

We have been unable to find a set of parameters resulting in even a qualitative fit to Kovacs data for the case II stochastic model described by eqs 10a,b. We currently have no physical reason as to why the case II form of the FPE is inappropriate. Subsequent discussion of predictions of the stochastic model will only be for the case I form of the model.

The values of parameters obtained as a result of optimization of the stochastic model are physically reasonable. The value of 2.84 nm for the size of the domain L is within the range estimated via NMR[35,36] and light scattering[41,42] studies discussed in the Introduction. It is amazing that by fitting macroscopic volume relaxation data, the experimentally determined size of the dynamic heterogeneity is recovered. It is also reassuring that the cooperativity parameter $z = 6.9$ from the overall fit of the stochastic model to the Kovacs data is consistent with the coordination number for a simple cubic lattice. Finally, the value of the slope of isomobility lines is close to the one for KAHR models, i.e., 1.43×10^{-4} g/(cm^3 K).

The predictions of the stochastic model were examined when the parameter L was made a linear function of temperature and specific volume, but this form of the stochastic model does not improve the quality of fit to the Kovacs data set in spite of the fact that there are two additional fitting parameters. This clearly indicates that one cannot assign the physical meaning to the domain size L in the stochastic model as a cooperativity length in the Adam−Gibbs[30] sense, because if this were the case one would have expected significant temperature dependence.

dx.doi.org/10.1021/ma300441a | *Macromolecules* 2012, 45, 7237−7259

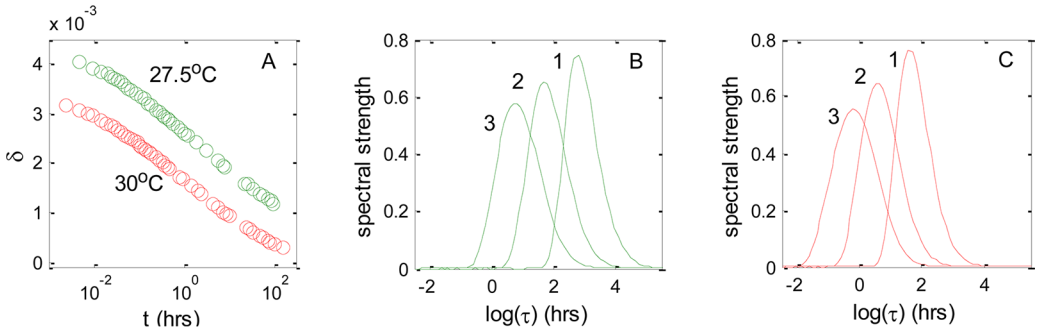

Figure 6. Stochastic model prediction of the thermorheological complexity in volume contraction experiment. (A) Kovacs data for volume response after down-jumps from 40 °C to indicated temperature; evolution of the spectrum after the down-jump to (B) 27.5 °C and (C) 30 °C. Numbers indicate snapshots of the spectrum taken at 3: $\delta = 3 \times 10^{-3}$; 2: $\delta = 2 \times 10^{-3}$; 1: $\delta = 1 \times 10^{-3}$.

Making the parameter s a weak function of temperature and volume, which results in curved isomobility lines in volume−temperature space, also does not improve quality of the fit to the Kovacs data set. It is significant that the key predictions of the stochastic model are due to the basic structure of the model and are not changed by the additional material parameters.

The key assumption of the traditional multimodal relaxation models such as KAHR is that the shape of the relaxation spectrum is constant, i.e., the material is thermorheologically simple. For the stochastic model developed in this paper there is no requirement of thermorheological simplicity, since there is only a single relaxation time. However, at any instant t_a the ensemble of domains will have an effective distribution of relaxation times which can be determined from the ME formulation of the stochastic model. From eq C.10 the normalized volume relaxation function for times t greater than t_a can be represented as a sum of exponential terms

$$\frac{V(t) - V_e}{V(t_a) - V_e} = \sum_{k=2}^{n} e^{\lambda_k (t - t_a)} g_k(t_a) \tag{24}$$

where the solution of the ME (see Appendix C) results in

$$g_k(t_a) = \frac{\sum_{i,j=1}^{n} Q_{ik} Q_{jk} \frac{\sqrt{p_i^{(s)}}}{\sqrt{p_j^{(s)}}} v_i (p_j(t_a) - p_j^{(s)})}{\sum_{m=1}^{n} v_m (p_m(t_a) - p_m^{(s)})} \tag{25}$$

where $\sum_{k=2}^{n} g_k(t_a) = 1$. We identify $\{g_k(t_a)\}$ as the instantaneous "spectrum" for the stochastic model with the relaxation times $\{\tau_k = -1/\lambda_k, k \geq 2\}$. Although λ_k's are not uniformly spaced, for the cases reported below with a large number of eigenvalues the spectrum in eq 25 provides an excellent representation of the instantaneous material response. In contrast to the multimodal KAHR model where the coefficients g_k are constant throughout the relaxation process, the $g_k(t_a)$ coefficients in the stochastic model change with t_a, i.e., the spectrum changes its shape—thermorheological complexity. The $\{\tau_k, g_k(t_a)\}$ spectrum determined via eq 25 can be thought of as the distribution an ensemble of domains would exhibit, where each domain is assigned a relaxation time $a(v_i)\tau_0$ and then the distribution along the time axis is determined—this is different from the distribution of volumes because of the strongly nonlinear relationship between the local volume and the relaxation time. If the current volume distribution does not deviate substantially from the equilibrium distribution, then the spectrum computed via eq 25 is reasonable; however, if the initial distribution is vastly different from the equilibrium distribution, then some of the $g_k(t_a)$ may turn out to be negative, indicating the limitations of "spectral" representation in eq 25.The instantaneous spectra computed using eqs 24 and 25 for the down-jumps from 40 °C to 30 and 27.5 °C are shown in Figure 6. For both down-jumps, the stochastic model predicts that the instantaneous relaxation spectrum shifts to longer times and narrows as the volume relaxation proceeds.

The shift to longer times is consistent with the traditional picture of physical aging, where the average relaxation time increases as the material densifies. The narrowing of the spectra indicates that those domains with the shortest relaxation time, i.e., the largest volume, age more rapidly than the meso-domains with longer relaxation times, thereby narrowing the spectrum. This simple explanation is not completely consistent with the SDE perspective of the stochastic model, since it implies that the identity of a fast relaxing site remains fast whereas in reality a single meso-domain can sample various mobility states. Nevertheless, in terms of the ensemble, those domains that are instantaneously in a high mobility state will on the average move more rapidly toward equilibrium than the low mobility domains, although the identity of just which domains are fast and which are slow changes during the course of the relaxation. The stochastic model provides a simple mechanism for the origin of thermorheological complexity.

However, the Kovacs down-jump curves shown in Figure 1A (with the exception of the smallest jump to 37.5 °C) have roughly the same slope and will superimpose when shifted along the time axes, giving the appearance that the response is thermorheologically simple. In contrast, the stochastic model predicts that the instantaneous relaxation times spectrum evolves during the course of the relaxation. How can the stochastic model that is inherently thermorheologically complex predict relaxation that appears to be thermorheologically simple? As shown in Figures 6B,C the shape of the effective spectra is essentially identical for the 30 and 27.5 °C down-jumps at the same δ. Since the instantaneous relaxation response depends upon the instantaneous spectrum, the macroscopic volumetric relaxation will be the same for both down-jumps, resulting in the appearance of thermorheological simplicity even though the underlying phenomenon is thermorheologically complex. The width of the instantaneous spectrum is quite narrow—of order 2 logarithmic decades; in contrast, the volume relaxation response of a single isotherm as measured by Kovacs[6] extends over four logarithmic decades, and if the isotherms are time−temperature shifted, the relaxation response occurs over at least 8 logarithmic decades. Thus, the shape of the volume relaxation predicted by the

dx.doi.org/10.1021/ma300441a | Macromolecules 2012, 45, 7237−7259

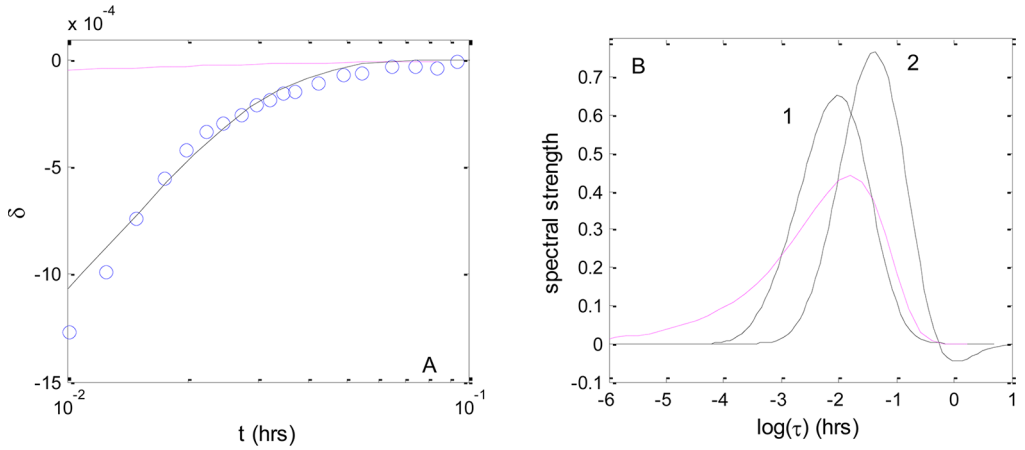

Figure 7. Prediction of the Kovacs "short anneal" experiment, i.e., volume response after temperature down-jump from 40 to 25 °C, annealing for 0.3 h, and temperature up-jump from 25 to 40 °C. (A) circles: data; solid line: Stochastic model prediction; blue line: KAHR model prediction. (B) Relaxation spectrum by the stochastic model: 1, at the beginning of the down-jump; 2, at the end of the up-jump. Blue line: relaxation spectrum employed by the KAHR model (optimized to fit the entire Kovacs data set).

stochastic model is primarily due to the movement of the spectra with time rather than excitation of different relaxation modes with vastly different time scales. This is a significantly different picture of structural relaxation than that implied by the multimodal KAHR model.

Short-Time Annealing Experiments. As discussed in the Introduction, KAHR-type models have difficulty in predicting the short annealing time experiments as shown in Figures 1E and 2A. This difficulty is surprising, because the thermal history is so simple, consisting of first quenching a sample from approximately T_g + 10 °C to T_g − 5 °C, annealing for a very short period of time, and finally rapidly reheating back to the original temperature. Nothing in this thermal history involves processes which could be difficult to model such as very long times when the physical aging is significant or a cooling to a temperature far below T_g where the validity of the extrapolation of the equilibrium log a data could be questioned.

However, the multimodal type models significantly underestimate the residual volume deviation after a short anneal thermal history as shown in Figure 2A, where even dramatic changes in the KAHR parameter values are unable to rectify the problem.

The stochastic model produces a qualitative improvement in the predictions shown in Figure 7A. In Figure 7B, the instantaneous relaxation spectra during the short anneal experiment are shown. The instantaneous spectrum immediately after the temperature jump back to 40 °C is shifted toward longer times and is noticeably narrower as compared to the spectrum at 40 °C just prior to the quench. The reason for the spectral narrowing is as follows: (1) When the down-jump occurs, the spectrum 1 immediately shifts to longer times. (2) The spectrum continues to shift to longer times as the material relaxes at 25 °C where the meso-domains with high mobility relax the most, thereby narrowing the spectrum. (3) Immediately after the up-jump back to 40 °C, spectrum 2 has the same narrower shape as just prior to the temperature up-jump. (4) With time spectrum 2 moves toward spectrum 1 that was present prior to the down-jump. The volumetric response predicted in Figure 7A is controlled by the instantaneous spectrum, which changes as spectrum 2 evolves to spectrum 1.

The relaxation times spectrum for the KAHR model is also shown in Figure 7B, where the KAHR model spectrum is much broader, with considerably more contributions from the short relaxation times. Now consider the evolution of the $\{\delta_i\}$ set in the KAHR model: (1) Initially all $\delta_i = 0$, since the material is at equilibrium. (2) After the down-jump the distribution is $\delta_i = -g_i\Delta\alpha\Delta T$, where $\{g_i\}$ are given by the KWW function; the shift to lower times is primarily governed by the temperature dependence of the log a function. (3) Since the annealing time at the lower temperature is very short, only the very fast relaxation processes can decay toward $\delta_i = 0$, and since the overall spectrum is shifted to longer times, even the faster relaxation process will not relax very much. (4) On the up-jump back to the original temperature the δ_i's associated with the slow relaxation processes (which were unable to relax) go to zero; however, the fast processes that have relaxed will exhibit small negative values. (5) The relaxation is very quick, since only the fast processes are nonzero, giving rise to the response predicted in Figure 7A. It is impossible to have the relaxations processes in the multimodal KAHR model that are fast enough to relax after the down-jump but still are slow enough after the up-jump to describe the short annealing experiments of Kovacs. The inability to predict the short time anneal experiments is a serious deficiency of the multimodal models, where the change in the shape of the effective spectra in the stochastic model is necessary to fit the data.

Memory Experiment. The stochastic and the KAHR models both predict the memory effect, but the origin is fundamentally different as shown schematically in Figure 8. First consider the stochastic model: (A) The instantaneous volume PDF for a material at equilibrium at the initial temperature above T_g, which is identical to the equilibrium PDF. (B) On the initial down-jump the equilibrium PDF shifts to smaller specific volumes, i.e., longer relaxation times, and the instantaneous PDF also shifts elastically to smaller specific volumes but keeps the same shape as PDF A. (C) The instantaneous PDF narrows as the faster relaxation processes with larger specific volume approach the equilibrium distribution more quickly, while the slower processes do not exhibit much of a change. (D) Immediately after the up-jump the narrow, instantaneous PDF C is shifted toward larger specific volumes, but the shape remains the same. The temperature of the up-jump has been

dx.doi.org/10.1021/ma300441a | *Macromolecules* 2012, 45, 7237−7259

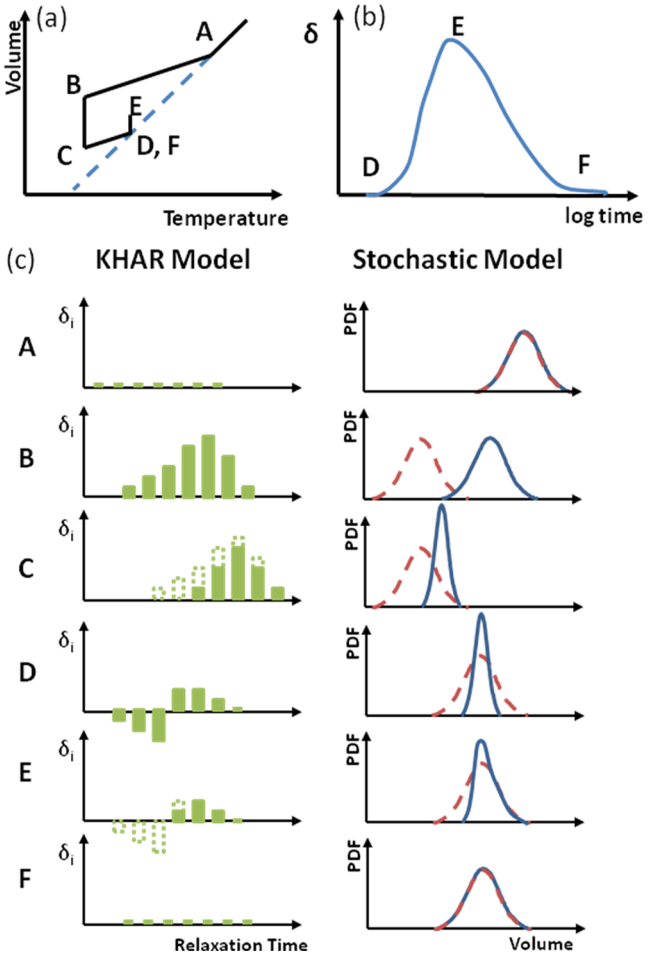

Figure 8. Schematic of the difference between the KAHR model and the stochastic model developed in this paper for the Kovacs memory experiment. The thermal history (a) and the evolution of the specific volume (b) for the memory experiment. The evolution of the δ_i spectrum for the KAHR model and the local volume probability density function (PDF) for the stochastic model are shown in (c). Red dashed line is equilibrium PDF, and blue solid line is the PDF predicted by the stochastic model. See text for explanation. For simplicity, the small changes in the width of the equilibrium PDF with temperature in (c) are not shown.

chosen so that the equilibrium PDF has the same average as the average of the instantaneous PDF. (E) The instantaneous PDF now becomes asymmetric, where (i) the fast relaxation processes at large volumes approach equilibrium first while the (ii) the slower relaxation processes at smaller specific volumes do not initially change. (F) Given sufficient time, the slower relaxation processes at smaller specific volumes eventually relax and the equilibrium distribution is recovered. The volume increase and subsequent decrease result from the increase in average volume shown in the PDF evolution from (D) to (E) followed by the decrease in the average volume in the PDF evolution from (E) to (F). Thus, the stochastic model predicts that the specific volume response in the memory experiment is due to the evolution of the shape of the volume distribution and the corresponding spectrum of the relaxation times.

The memory effect for the KAHR model is also illustrated in Figure 8, where the origin of the memory response is quite different. Specifically: (A) At equilibrium the value of the individual order parameters δ_i are zero. (B) After the first temperature jump in the memory experiment thermal history, the order parameters have the values $\delta_i = -g_i\Delta\alpha\Delta T$, and the temperature dependence of log a shifts the whole spectrum toward longer relaxation times. (C) The $\{\delta_i\}$ distribution begins to evolve, where the δ_i's associated with the faster relaxation processes relax first. (D) The up-jump to the second temperature causes the δ_i's associated with the faster relaxation processes that had already relaxed to become negative because of the instantaneous shift $\delta_i = -g_i\Delta\alpha\Delta T'$ and $\Delta T'$ is positive. In contrast, for the slower processes where the δ_i's did not relax, there is a reduction in the magnitude of the δ_i's. Since the specific volume immediately after the up-jump is equal to the equilibrium volume, the area under the positive δ_i's minus the area above the negative ones must equal zero. (E) The fast processes rapidly relax to $\delta_i = 0$; consequently, the sum of the remaining δ_i's will be positive, resulting in an increase in the specific volume. (F) With sufficient time all of the $\{\delta_i\}$ order parameters relax to zero, and consequently the specific volume now decreases to equilibrium. The evolution of the δ_i's spectrum from (D) to (E) to (F) is the origin of experimentally measured specific volume in the memory experiment in the KAHR model.

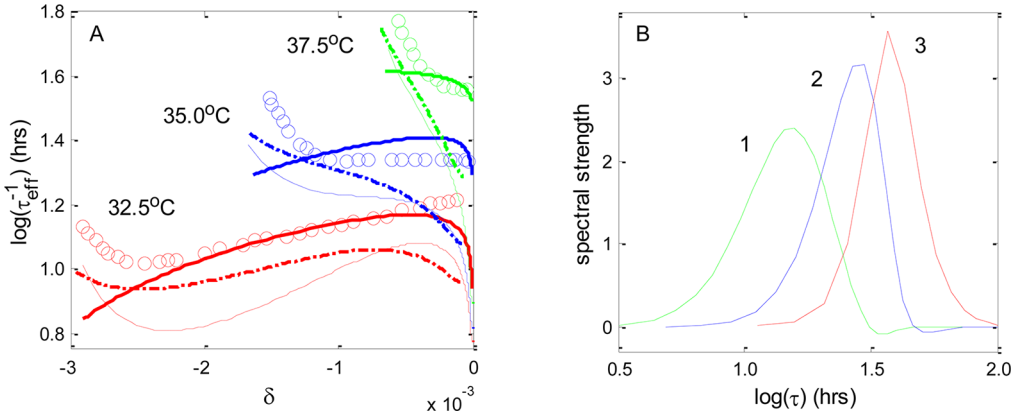

Figure 9. Prediction of the "expansion gap" effect, i.e., volume response after an up-jump from indicated temperature to 40 °C. (A) τ-effective behavior as volume (described by the deviation δ) relaxes toward equilibrium; circles: data; light solid line: KAHR model prediction; dash-dotted line: stochastic model prediction using the parameter set optimized over the entire Kovacs data set; solid line: stochastic model prediction using the parameter set optimized to fit specifically this τ-effective data (L = 9.7 nm, z = 1.7). (B) Relaxation spectrum resulting from the stochastic model (L = 9.7 nm, z = 1.7) calculated at $\delta = -2 \times 10^{-4}$ for the temperature up-jump from (1) 37.5, (2) 35, and (3) 32.5 °C.

dx.doi.org/10.1021/ma300441a | Macromolecules 2012, 45, 7237−7259

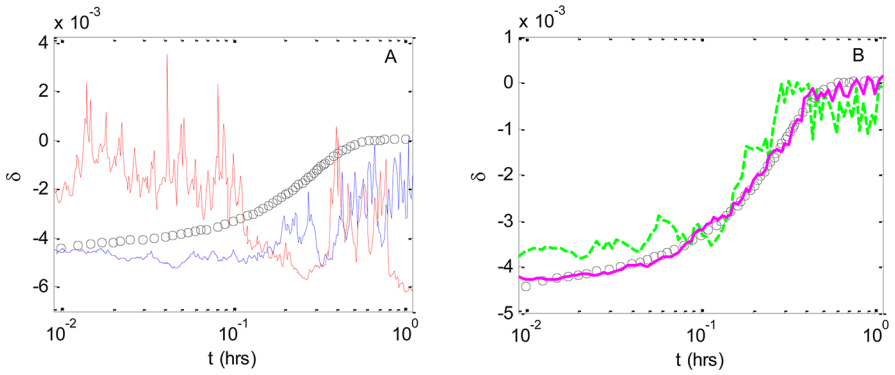

Figure 10. Stochastic model prediction of the Kovacs up-jump from 30 to 40 °C experiment. Circles: data. (A) Examples of two realizations: solid lines, where one realization (blue) started from the macroscopic equilibrium volume and the second realization (red) started a specific volume greater than the macroscopic volume. (B) Average over 300 realizations: dotted line; average over 3000 realizations: thick solid line.

The origin of the memory effect as predicted by the KAHR model is quite different from that predicted by the stochastic model. In the KAHR model all relaxation times are affected equally by the macroscopic specific volume, where the individual δ_i's are the order parameters that sum to the macroscopic δ. Carefully examining Figures 8D,E for the KAHR model, the δ_i's that are negative relax first and those that are positive relax last. This highlights the fact that the δ_i's are just formal parameters devoid of clear physical meaning; otherwise, were they truly components of the total specific volume, one would think that a process with a positive δ_i, and hence a large effective volume, would relax first. In contrast, the origin of the memory effect in the stochastic model is more physically appealing, since it predicts that regions of larger specific volume relax more rapidly than regions of smaller specific volume. In our opinion, the predictions of the memory experiment by the multimodal class of models such as KAHR is fortuitous, where more complex multistep temperature jumps would potentially show qualitative disagreement.

Predictions of τ_{eff}. The τ_{eff} plot in the Kovacs data set is particularly difficult to predict, where even if a fit appears reasonable in "normal" coordinates, i.e., δ versus log t, it can still deviate dramatically in the τ_{eff} plot because the latter magnifies the region close to $\delta = 0$ (see discussion in McKenna et al.[15]). It is well-known that the KAHR-type models are incapable of predicting the so-called expansion gap[27] as is shown in Figure 9A for the model already described in association with Figure 1.

As shown in Figure 9A, the stochastic model also cannot describe the expansion gap using the optimized parameter set given in Table 1. However, if only the data in the τ_{eff} plot are included in the parameter optimization, then the stochastic model can describe the significant difference in τ_{eff} at very small δ, which is the key feature of the expansion gap. The $\{L, z\}$ pair needed for the improved predictions shown in Figure 9A is (9.7 nm, 1.7), which is significantly different from the (2.8 nm, 6.9) parameter set used previously. Although this new choice of parameter values worsens the quality of the fit for the other thermal histories, the stochastic model has a structure that at least in principle is able to capture the expansion gap. We believe that this is the first time that the expansion gap has been successfully predicted by any model.

The reason that the stochastic model is able to qualitatively predict the expansion gap is as follows: For the expansion gap effect to occur some feature in the model must still strongly depend on thermal history even when the average volume is near equilibrium value. In Figure 9B, we have focused on the evolution of the stochastic model's effective relaxation spectrum $g_k(t_a)$ from eqs 24 and 25 at the final stages of the relaxation, i.e., at the δ equal -2×10^{-4}. The stochastic model predicts that the location and shape of the spectrum exhibit a strong dependence on thermal history, even though the temperature and specific volume are nearly the same. This again illustrates that the evolution of the shape of the spectrum, which is an inherent feature of the stochastic model, is what controls the experimentally observed specific volume response. In contrast, for multimodal relaxation models the shape of the spectrum remains constant and the latest stages of relaxation are governed simply by the order parameter with the longest relaxation time regardless of thermal history; hence, all τ_{eff} curves rapidly converge into a response corresponding to this longest relaxation time. In summary, the structure of the stochastic model offers the possibility that eventually it may be possible to fit the Kovacs data set including the expansion gap, but this will require improvement in the stochastic model.

Fluctuations in a Single Mesoscopic Domain. The fit to the Kovacs data set was done using the ME form of the stochastic model, which is equivalent to an ensemble average of the SDE form of the model. The predictions of selected realizations of the SDE form of the stochastic model (i.e., eq 8) with the same model parameters used to fit the Kovacs data are shown in Figure 10 for a simple up-jump from 30 to 40 °C. An individual meso-domain experiences extremely large fluctuations in volume, i.e., δ changes of $\pm 4 \times 10^{-3}$ which are larger than the overall macroscopic δ changes of 4×10^{-3}.

Examining a single realization, it is difficult to discern the type of volume relaxation occurring macroscopically. Even though individual realizations do not exhibit discernible trends, the ensemble average of a number of independent realizations does exhibit the anticipated macroscopic relaxation response as shown in Figure 10B where an ensemble of 1000 or more realizations is needed to begin to recover the macroscopic response. The ensemble averages shown in Figure 10B clearly demonstrate that the SDE form of the stochastic model, and the FPE/ME forms are consistent. The individual realizations shown in Figure 10A provide a better picture of the local glassy state than the average picture that is given by the Kovacs experimental data. Since the local mobility, i.e., log $a(v,T)$, is a strongly nonlinear function of the specific volume as defined in eq 23, the relaxation time associated with density fluctuations in Figure 10A experiences mobility fluctuations over 6 orders of magnitude. Thus, the stochastic model as formulated here

dx.doi.org/10.1021/ma300441a | *Macromolecules* 2012, 45, 7237−7259

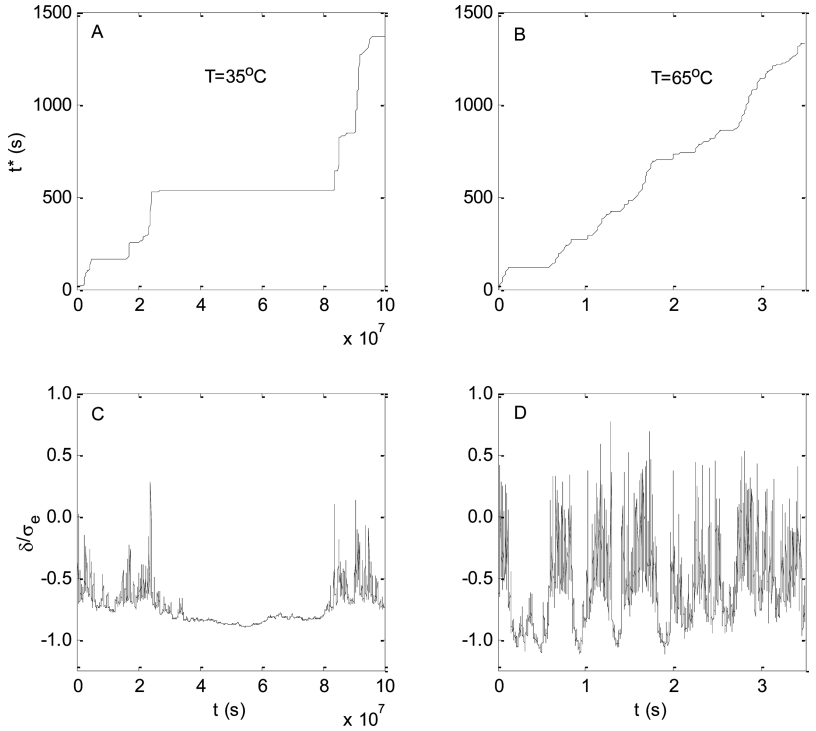

Figure 11. Stochastic model prediction of (A, B) the evolution of the material time t^* in a single domain in equilibrated state at temperatures indicated, where the corresponding volume behavior is shown respectively in (C, D).

exhibits mobility fluctuations consistent with the qualitative picture of dynamic heterogeneity of glassy materials emerging from the experiments.

The material time[76,77] t^* is a useful way to consider the time scale for relaxation for a process undergoing a complex thermal/deformation history

$$t^* = \int_0^t \frac{d\xi}{a(\xi)} \tag{26}$$

A number of nonlinear constitutive equations for polymer glasses have been built using t^* (see Caruthers et al.[24] for details), where the $a(t)$ shift factor depends upon macroscopic quantities such as the specific volume, stress, configurational entropy, and configurational energy. The material time t^* can also be used for an individual meso-domain, but the local mobility as defined in eq 26 should be employed where the local specific volume is determined from a realization of the SDE. Consequently, the "local material time" t^* is also stochastic, where the macroscopic material time is the ensemble average over many SDE realizations.

The evolutions of t^* are shown in Figure 11 for a material that is macroscopically at equilibrium for two temperatures: one near the glass transition (T = 35 °C) and another well in the liquid state (T = 65 °C). As expected, the same amount of relaxation at the lower temperature takes roughly 10^7 times longer than at the higher temperature. More significantly, the evolution of the material time is qualitatively different at these two temperatures. For a representative meso-domain well above T_g, t^* changes at nearly a constant rate (i.e., Figure 11B), where the slope corresponds to the average shift factor $\langle a(v,T)\rangle$ even though there are significant fluctuations in the specific volume (i.e., Figure 11D). In contrast, at the lower temperature a given domain generally exhibits periods of time with little or no relaxation that is randomly punctuated with a sudden burst in the relaxation (i.e., Figure 11A) associated with large positive fluctuations in the specific volume (i.e., Figure 11C).

Note that it may appear that average value of volume fluctuations shown in Figure 11C is not at zero, but negative; however, this is an erroneous impression due to the discreteness of the time points. Specifically, when the domain makes an excursion into the region of large positive values, it bounces back within such a short time that the whole event is undetected on the time scale used for plotting. Although not seen in the Figure 11C,D, these large positive values of volume provide an important contribution when the average is evaluated ensuring that its value is where it is supposed to be i.e. exactly at zero.

The response in Figure 11A indicates that the stochastic model predicts that when the material is below T_g a given domain will remain frozen for a long period of time and then undergo a rapid change in mobility after which it will return to its frozen state. If one performs an ensemble average of the low temperature t^* vs t realizations, a straight line emerges with the appropriate slope of $\langle a(v,T)\rangle$, although the response of an individual domain is anything but linear. In summary, the stochastic model predicts that in the liquid state every meso-domain experiences nearly the same volume/mobility history, which is approximately the same as the macroscopic response. In contrast, the response of a meso-domain in the glassy state is basically quiescent with randomly spaced events of very rapid relaxation, where the responses for different domains are quite different and bear no resemblance to the smooth, linear response exhibited macroscopically as determined via an ensemble average.

IV. DISCUSSION

Features of the Stochastic Model for Volume Relaxation in the Glass Transition Region. A stochastic

dx.doi.org/10.1021/ma300441a | Macromolecules 2012, 45, 7237−7259

model for structural relaxation in glasses has been developed that acknowledges the fluctuations associated with the dynamic heterogeneity in polymeric glasses. Three key model assumptions are (i) potentially complex spatial coupling between neighboring meso-domains is simplified using a mean field approximation, (ii) the local dynamics of the meso-domain are inherently a single Debye process, and (iii) the local dynamics are assumed to be a function of the local density with a form that is consistent with the macroscopic mobility vs temperature data. This picture that the mobility character of a given region of space changes with time is consistent with data from multidimensional NMR experiments.[34,36]

A major feature of the stochastic model is that it only employs a *single* relaxation time; however, the model predicts that the macroscopic volume relaxation will occur over many logarithmic decades of time consistent with experimental observations. A consequence of the small size of the meso-domains (i.e., 2−3 nm) is that the specific volume fluctuations are large; thus, an individual meso-domain samples a wide range of mobility states because the log $a(v,T)$ shift factor is a highly sensitive and nonlinear function of specific volume. Because there is no spectrum of relaxation times, the stochastic model does not assume (i) the shape of the spectrum or (ii) that the shape of the spectrum remains constant as the macroscopic temperature and/or specific volume is changed. The stochastic model predicts that the apparent relaxation spectrum as computed from instantaneous distribution of specific volumes will change its shape, i.e., narrow or broaden, during the course of a relaxation experiment. The appearance of thermorheological complexity in polymeric glasses has been observed by Plazek,[75,78] where the stochastic model provides a rational explanation for the origin of the thermorheological complexity.

An important caveat is that the form of the relaxation equation given in eqs 8 and 9 implies that at the meso-domain level the relaxation process is inherently a Debye process with a single-exponential relaxation time. At the same time there are experimental observations[79] suggesting that the elementary glassy dynamics is inherently nonexponential. Although mathematically involved, it is possible to replace eq 9 with a more complex form that would result in a stretched exponential response at the mesoscopic level. However, such an extension is well beyond the goal of this communication, which is to determine if Kovacs volume relaxation data can be described with the simplest model that assumes (i) dynamic heterogeneity and (ii) the local relaxation being a simple Debye process.

There is nothing in the stochastic model that is specific to PVAc; thus, the underlying material response for all glass formers is predicted to be thermorheologically complex. However, time−temperature superposition with the implication of thermorheological simplicity is observed in a wide variety of relaxation experiments for a large number of low molecular weight and polymeric glass-formers, although some very careful measurements in the glass transition region question the assumption of thermorheological simplicity.[75,78] The resolution of why a material that is thermorheologically complex exhibits apparent thermorheological simplicity is as follows: although the shape of the spectrum changes during the course of the relaxation, for large deviations from equilibrium the dominant influence on all relaxation times is the average value of the mesoscopic density (or any other structural variable that controls the relaxation), rendering insignificant any dependence on higher moments of the structural variable distribution. However, as the average deviation approaches zero, the fine structure of the structural variable distribution (and, hence, the relaxation time spectrum) becomes important and the appearance of thermorheological simplicity is lost. The shape of the distribution is sensitive to thermal history, where a system might arrive at the same average volume, but with dramatically different distributions of the relaxation times. For example, the final approach to equilibrium for the Kovacs down-jumps (Figures 1A and 5A) the isotherms do not superimpose for δ less than 1×10^{-3}. This implies that to observe thermorheological complexity more clearly one has to focus on the region of small deviations from equilibrium, where the accuracy of measurements rapidly deteriorates. For very accurate measurements such as those by Plazek[75,78,80] on the shear creep compliance in the glass transition region for polystyrene, PVAc, and other materials, the violation of thermorheological simplicity was clearly observed.

Comparison of Stochastic Model with the Multi-Modal KAHR Model. The stochastic model was fit to the whole Kovacs data set for volume relaxation of PVAc[7], where the overall fit to the whole data set was very good. The overall fit of the multimodal KAHR[18] was also quite good for most of the data; however, the KAHR model is unable to predict two features of the Kovacs PVAc data: (i) short time annealing experiments and (ii) the τ_{eff} data (see Figure 2). The KAHR model is unable to describe these experiments even if it is optimized to just that part of the Kovacs data set. The stochastic model naturally predicts the short annealing time response (see Figure 7), where the change in the shape of the effective spectrum is what enables the stochastic model to describe the data. The stochastic model was also able to describe the Kovacs τ_{eff} data, although this required a different set of model parameters than that used for predicting the rest of the Kovacs PVAc data set. The key feature of the stochastic model that enables prediction of τ_{eff} is that the tails of the distribution can evolve in different ways even though the experimentally measured specific volume is constant, and the tails of the distribution can have a significant effect on the ensemble average of the mobility (i.e., τ_{eff}). Since a different set of model parameters were required to fit the τ_{eff} data, the stochastic model in its current form is not complete. Nevertheless, the structure of the stochastic model shows promise, since for the first time there is a prediction with a mechanistic explanation of the origins of longstanding challenge of modeling Kovacs' τ_{eff} data.

Even when the stochastic model and the multimodal models like KAHR both predict the experimental data there are significant differences when one examines the inner details of the predictions. As an example consider the memory experiment, where both models do a reasonable job of describing the Kovacs memory data. The stochastic model predicts the increase and subsequent decrease in the specific volume during a memory experiment as a consequence of (i) a narrowing of the mesoscopic specific volume distribution that has occurred during aging at lower temperature followed by (ii) a broadening of the specific volume distribution at the final temperature (see Figure 8). These predictions are consistent with the idea that domains with larger specific volume and hence larger mobility will relax first. In the memory experiment the KAHR model predicts that the processes with negative δ_i's

relax first followed by processes with positive δ_i's, which emphasizes that the δ_i's are just formal parameters.

The stochastic model has four parameters, of which two are strongly correlated, that were optimized from the Kovacs data: s, τ_0, and the $\{L, z\}$ set. The KAHR-like model has three optimized material parameters: the KWW parameter β, the Narayanaswamy parameter x, and τ_0. The KAHR parameter $\theta_T = 2.303\ c_1/c_2$ is fixed by the equilibrium log a vs temperature data, which considering the quality of data as shown in Figure 4 would seem to be a basic requirement of any structural relaxation model. We note that in the original KAHR model[18] the relaxation spectrum was not assumed to be a KWW function, but rather a box distribution of relaxation times, although the basic formulation does not require any specific shape of the distribution. We have performed simulations with both the KWW and box spectra, where both spectral shapes result in very similar predictions. It might be possible to improve some features of the KAHR model by adjusting the shape of the relaxation spectrum; however, this would increase the level of parametrization. However, the ability to describe the short time annealing and τ_{eff} data cannot be resolved by changing the shape of the spectrum—it requires that the spectral shape change during the experiment. In summary, both the KAHR and stochastic model have effectively the same number of model parameters; thus, the improvement in data fitting by the stochastic model is not due to additional model parameters. More important than the number of parameters is the fact that the stochastic model avoids the need to determine the shape of spectrum.

The KAHR class of models typically assumes a linearized form of log a using θ_T. We have also fit the Kovacs volume relaxation data using the nonlinear form of log a given by eq 20 with the KWW form for the relaxation spectra in the multimodal model; however, there were the same shortcomings for the short time annealing and the τ_{eff} experiments. We have also used a linearized version of eq 23 for log a in the stochastic model; specifically

$$\log a(v, T) = -\frac{c_1}{c_2}(T - T_g) - \frac{c_1}{c_2}\frac{\frac{1}{z}v + \frac{z-1}{z}V - V_0(T)}{V_g\alpha_1 - s} \tag{27}$$

In contrast to the linearized KAHR model, the predictions of the stochastic model using the linearized version of log a are much worse. This result is not surprising, since the average volume changes explored in the Kovacs experiments are relatively small; in contrast, the mesoscopic volume in the stochastic model fluctuates over a much wider range, where the linearized log a expression is apparently inadequate. Thus, the differences between the predictive capabilities of the stochastic vs multimodal model are not due to the linearization of log a used in the multimodal model. However, the fact that the nonlinear form of log a is significant in the stochastic model raises the question if a nonlinear expression other than eq 23 were employed could it further improve the fit to the Kovacs data set.

Comparison to Robertson et al. Fluctuation Model. The stochastic model developed in this paper is closely related to the model of Robertson, Simha, and Curro (RSC).[20] RSC employed a ME formulation, where the rate of relaxation of the discretized volume distribution is controlled by the current value of the local fractional free volume, f, in the Simha–Somcynsky (SS) equation-of-state that is determined using the instantaneous T and v. In the model development in this communication, the point of departure was the SDE, which we believe more clearly exposes the underlying physics of the process and also more clearly enables the future development of improved models that include fluctuations, where the ME form was just used as a computationally efficient algorithm for solving the associated FPE. Irrespective of one's perspective on whether the SDE, FPE, or ME is the most intuitive point of departure, the three formulations are mathematically equivalent, assuming the level of discretization in the ME formulation is sufficient. A key question is: why did the RSC fail to produce fits to the Kovacs data set of the quality presented in this paper if the structure of the RSC and stochastic model are similar?

Using the equilibrium relationship $f_e(T) = f_g + \tilde{\alpha}(T - T_g)$ with the WLF equation, RSC developed the following equation

$$\log a = -c_1 + c_1\frac{c_2\tilde{\alpha}}{c_2\tilde{\alpha} + f(T, V) - f_g} \tag{28}$$

where $f_e(T)$ was replaced with $f(V,T)$ determined from the SS equation of state and f_g is the fractional free volume in the reference state of $T = T_g$ and $P = 1$ atm. In a series of papers Vlesshouwers and Nies (VN)[21,22] used the fraction $f(v,T)$ obtained via the Holey Huggins (HH) equation of state, but employed the rest of the RSC framework. Although the RSC model and the more recent VN variation are structurally similar to the stochastic model developed in this paper, their ability to quantitatively describe the whole Kovacs data set is disappointing. As an example, the RSC and VN models cannot describe the simple down-jumps from 40 °C to various temperatures (in their original paper RSC attempted to alleviate the problem by making τ_0 temperature dependent). In order to address this deficiency, in later publications[29] RSC made additional assumptions employing different log a functions below and above certain temperature, but the results were only marginally improved.

The difference in the descriptive power of the current stochastic model and the RSC model is due to the form of log a. Equation 28 does not contain any adjustable parameters, since c_1 and c_2 are determined by the log a vs temperature data above T_g and the parameters contained in the SS or HH equation-of-state used to specify $f(v,T)$ are determined from the PVT behavior of the polymer. Although the temperature dependence of log a along the $P = 1$ atm line for an equilibrium material is the same for the stochastic model and the RSC or VN models, the volume dependence is different, and since volume fluctuations are quite large, the effect of the different assumptions concerning the v-dependence of log a is significant.

The ratio of the relaxation time used in the stochastic model (using the parameter values from Table 1) and the relaxation time of the RSC model is shown in Figure 12 as a function of the specific volume deviation δ. Since the RSC results were in terms of the fractional free volume, we have recalculated all the expressions in terms of the specific volume using the SS equation of state with the parameters employed in the RSC paper. Results for two temperatures $T = 40$ °C and $T = 25$ °C are presented. The values of the logarithm of the ratio of the relaxation times near zero indicate the regions where the two models display similar behavior and, hence, where the RSC model should be expected to describe the Kovacs data well similarly to the stochastic model. The agreement between

dx.doi.org/10.1021/ma300441a | Macromolecules 2012, 45, 7237–7259

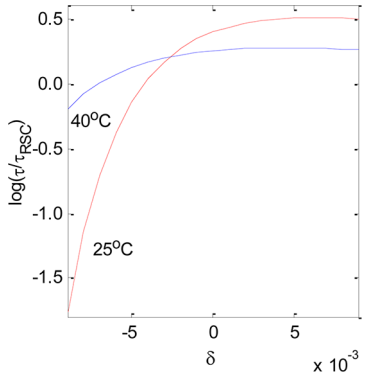

Figure 12. Comparison between the expressions for the relaxation time (as a function of temperature and volume) in the present communication (τ) and in the paper by Roberson et al. (τ_{RSC}).

models is better at higher temperature in the region of the negative δ's; thus, it is not surprising that up-jumps to 40 °C is the type of thermal history best described by the RSC model. However, for down-jumps to 25 °C (large positive δ's) the RSC relaxation time is much too fast and the prediction is the poorest. An important observation resulting from Figure 12 is that the RSC predictions cannot be improved through an adjustment of τ_0, which would correspond to a vertical shift of the curves in the figure. Indeed, the prediction of the down-jump experiments can be improved considerably using such procedure, but at the expense of the prediction of the up-jumps owing to the curvature of the dependencies in Figure 12.

The dramatic change in the dependence of relaxation times observed for the RSC model for large negative δ's is probably due to using of the SS equation of state to determine free volume and hence mobility.

There are a number of other implicit assumptions made in the RSC model and VN variation which we address in detail in the Supporting Information that are also detrimental to the quality of the fit to the Kovacs data, but they are secondary in effect as compared to the above-mentioned deficiency of the log a function. The basic structure of the model developed by RSC has the capability of describing the Kovacs data set; however, the v-dependence of log a is tied to a particular equation-of-state that results in a wrong volume dependence of the mobility.

Formulation of the Stochastic Model. As is clearly shown by the SDE form of the stochastic model, the current modeling effort is a first step toward introducing fluctuations into continuum mechanics. This is a major departure from the traditional continuum mechanics, where all temporal and spatial fluctuations are averaged. Traditional continuum mechanics has a solid thermodynamic foundation.[81,82] Also, the theory of fluctuations emerges from the theoretically sound, full phase space description of discrete molecules. However, the proposed approach falls in between traditional continuum mechanics and statistical mechanics. Care must be taken to ensure that there is no violation of the basic principles of continuum physic including the Second Law. The first step toward this will require the development of a full tensorial description that allow for imposition of the requirements of conservations of mass, momentum, and the Second Law. There are additional assumptions as well. It was assumed that the fluctuations are Gaussian even for large departures from equilibrium, although there is no reason that the tails of the distribution have to behave in a Gaussian manner. The form of $B(v,T)$ given in eq 9b was determined in order to satisfy stationarity at equilibrium, where the same form of $B(v,T)$ was also used for nonequilbrium states. Is this assumption valid? The objective of this paper is not to address these significant concerns, but to indicate that there appears to be significant value in considering the addition of fluctuations—value that can justify the investment of effort to address the questions above.

A significant caveat needs to be mentioned. The stochastic model developed in this paper has assumed that the mobility is controlled by mesoscopic density fluctuations; consequently, the magnitude of these fluctuations is solely determined by the requirement that the model describe the volume relaxation data. However, there are other attractive candidates for the mobility relationship including configurational entropy,[52] configurational internal energy,[24] stress,[83] etc. Moreover, the model has assumed that the mesoscopic deformation is purely isotropic, where mesoscopic fluctuations are most certainly anisotropic. If the assumptions of either the form of the mobility relationship (e.g., eq 23) or isotropic mesoscopic deformation are not valid, then these errors have been subsumed into the parameters that control the magnitude of the density fluctuations. Thus, one must be careful at this early stage of model development not to place too much emphasis on volume fluctuations, since they may be a surrogate for a more fundamental quantity that controls the local mobility. The key issue is that fluctuations must be included in modeling the glassy state.

The stochastic model has employed a mean field approximation, where a single domain of size L is imbedded in a continuum that has the ensemble average properties. This approach completely ignores correlations between neighboring domains. The ability of the stochastic model to accurately predict the extensive Kovacs data set with only three model parameters indicates that this mean-field approximation is not unreasonable at least for the small isotropic macroscopic volume changes under consideration. For large anisotropic deformations the mean-field approximation will need to be carefully examined.

Implicit in the stochastic model is the requirement that only the local volume v controls the rate of relaxation in the FPE. However, in order to fit the data the rate expression in eq 23, also included the ensemble average volume given by

$$V(t) = \int_{-\infty}^{\infty} dv'\, v' p(v', t) \tag{29}$$

Is this modification of the FPE appropriate? This is a valid concern since the derivation of the stochastic model was based on the relaxation rate depending on just the stochastic variable and not also on an ensemble average of this variable. We give no formal proof (see ref 84); however, the numerical simulations of the SDE using the combination of v and V clearly show that the form of the drift term A and the diffusive term B given in eqs 9 with the rate calculated via eq 23 does result in the stationary distribution given in eq 7.

Connection of Stochastic Model to Other Experiments and Simulations. The stochastic model qualitatively describes the time development of the width of the distribution of volume fluctuations after step changes in temperature observed in some inorganic glass formers by light scattering.[39] The model predicts the experimentally observed maximum (minimum) in the variance of the fluctuations of the specific volume $\langle \delta v^2 \rangle$ following up-jumps (down-jumps) in temper-

ature. This behavior is a natural consequence of the broadening/narrowing of the probability density function of the local volume, where the high volume portion of the volume distribution relaxes toward its equilibrium faster than the low volume portion. Thus, for up-jumps in temperature there is an initial broadening of the volume distribution as the larger volumes of the distribution increase faster than the lower volumes. In contrast, for down-jumps there is an initial narrowing of the distribution as the larger volumes of the distribution decrease faster than the smaller volumes.

The SDE form of the stochastic model predicts large volume fluctuations for a realization of a single domain during a given thermal history. This presence of large fluctuations in the molecular properties of a glass such as local shear modulus[85] are well-known in molecular simulations, where recent work[86] showed that the fluctuations in the molecular stress, etc., seem to become relevant for the macroscopic mechanical behavior when averaged over a local domains of sizes that begin to approach the 2−3 nm, i.e., the size predicted by the stochastic model and measured by NMR.[36] At this time we are not making any direct comparison with the magnitude of fluctuations predicted by the stochastic model and molecular dynamics simulations, and as discussed above, specific volume may not be the appropriate quantity to compare with molecular simulations. However, the stochastic model provides a potential framework to gain further insight from molecular simulations; specifically, current simulations either use very large systems or ensemble average their predictions in order to reduce fluctuations so they can be compared with experimental data. In contrast, the stochastic model uses fluctuations and makes very clear predictions about how the distribution of a fluctuating variable evolves during a macroscopic experiment. Although well beyond the scope of this paper, the stochastic model (and its future extensions) can potentially provide a continuum framework that takes better advantage of the extensive fluctuation information that is contained in molecular dynamic simulations of the glass.

Limitations of the Current Stochastic Model. The current formulation of the stochastic model has a number of clear limitations. In this paper the model was used to predict the Kovacs data set[7] which was all at 1 atm pressure; however, the model makes predictions at other pressures. The effect of pressure is controlled by the log $a(V,T)$ surface shown in Figure 3. To first order T_g occurs when log a equals zero; thus, $T_g(P)$ is controlled by the slope s of the isomobility lines in $V-T$ space, where s is one of the parameters determined by optimization of the 1 atm Kovacs data. If the optimized s resulted in the log a contours shown in Figure 3B, then the pressure dependence of T_g would have been predicted; however, the optimized s results in the contours shown in Figure 3A, which gives a qualitatively incorrect $T_g(P)$. The $T_g(P)$ discrepancy cannot be fixed by any change to the current stochastic model that assumes that mobility is controlled by the local specific volume. This conclusion forces the consideration of a generalization of the current model to use an alternative mobility variable such as configurational entropy, which will be the subject of a future communication where multiple fluctuating variables (e.g., volume and entropy) must now be considered. Notwithstanding the inability of the current version of the stochastic model to predict $T_g(P)$, the current model has provided considerable value, since (i) the structure of the approach to include fluctuations is best exposed in its simplest form and (ii) it can describe the extensive Kovacs data set using a single relaxation time—not an inconsiderable task.

A second limitation of the model is that it currently applies only to isotropic deformations. Moreover, even in deformations that are macroscopically isotropic the local domain can experience anisotropic fluctuations. It will be necessary to develop a full tensorial approach that includes fluctuations in order to determine if including fluctuations can provide insight and improved predictions for the complex nonlinear relaxation behavior that is observed for glassy polymers. The isotropic model developed in this paper provides the point of departure for future development of a full tensorial description.

V. SUMMARY

A single relaxation time model that includes fluctuations has been developed to describe the volumetric relaxation response of a glassy material, where the rate of local relaxation is controlled by the local state variable which for this model is the local specific volume. The incorporation of fluctuations in the stochastic model directly acknowledges dynamic heterogeneity that is well established experimentally for glass forming materials. Three different, but mathematically equivalent, forms of the stochastic model have been developed: (i) the stochastic differential equation (SDE) that provide a realization of the evolution of the specific volume including fluctuations in a local mesoscopic region, (ii) the Fokker−Planck equation (FPE) that describes the evolution of the probability density of the local specific volume, and (iii) a master equation (ME) that is a discretized version of the FPE that is useful for numerical solutions. The stochastic model developed in this paper has four model parameters (two of which are strongly correlated) which were optimized for the extensive poly(vinyl acetate) volume relaxation data of Kovacs.[7] The single relaxation time stochastic model does an excellent job of fitting the entire data set. Since the stochastic model only has a single relaxation time, there is no need to postulate/determine the shape of the relaxation spectrum as required by the traditional multiple order parameter models. The stochastic model results in an inherently thermorheologically complex material, although for appropriate thermal histories it predicts relaxation responses that can be operationally shifted along the log time axis to effect superposition. However, for relaxation phenomena that are close to equilibrium, the stochastic model predicts a thermorheologically complex relaxation response in agreement with experimental observations. This is the first model that naturally predicts thermorheological complexity.

The stochastic model does a better job than the existing multirelaxation time models in predicting the whole Kovacs data set. The stochastic model can describe the τ_{eff} expansion gap, although it requires a significantly different set of model parameters than the parameters needed to describe the rest of the Kovacs data set, indicating that some features of the stochastic model may be needed to resolve the τ-effective paradox. Also, the stochastic model does not predict the pressure dependence of T_g. These failures suggest that some essential physics is still missing. There are two obvious places in the formulation of the stochastic model, which might have caused aforementioned problems: (i) the assumption that volume is the critical variable controlling mobility in the glass transition region, where there are other plausible candidates including configurational entropy and configurational internal energy, and (ii) the assumption that the local domain can only deform isotropically, when the only requirement is that the

ensemble average of the local responses be isotropic. Notwithstanding, the difficulties with respect to τ_{eff} and $T_g(P)$, the current version of the stochastic model does an excellent job of predicting the rich, nonlinear set of Kovacs PVAc volume relaxation using effectively three material parameters and without needing a relaxation time spectrum. The stochastic model clearly demonstrates the value of incorporating fluctuations in models for glassy polymers and exposes the mathematical structure of this class of model.

APPENDIX A. DERIVATION OF THE SDE

In this Appendix the deterministic relaxation equation will be generalized to include fluctuations, where the volume relaxation equation (i.e., eq 5) is a relevant example. For mathematical simplicity the relaxation rate, $R(v)$, is employed rather than $1/a(v,T)\tau_0$, and the temperature dependence is omitted. Hence, the problem is formulated as follows: given a deterministic nonlinear ODE of the form

$$\frac{\mathrm{d}}{\mathrm{d}t}v = -R(v)(v - V_e) \tag{A.1}$$

construct a stochastic generalization of eq A.1 with a stationary solution $p^{(s)}(v)$ that is consistent with the equilibrium thermodynamics one given by eq 7. The stationary distribution given in eq 7 is Gaussian, and we will assume this is the functional form in the subsequent treatment; however, the Gaussian assumption is not critical to the analysis. In addition, the stochastic generalization of eq A.1 must limit to the deterministic ODE given in eq A.1 in the case of vanishing fluctuations. An important issue will be to determine the uniqueness of the stochastic generalization of the deterministic relaxation equation.

The problem defined in the previous paragraph is different than the one traditionally considered in statistical mechanics. The traditional objective is to determine the stationary distribution for a system with a given systematic generalized force (i.e., the right-hand side in eq A.1), when the fluctuations are described via a diffusive-like term with a constant diffusion coefficient D. In the standard approach,[54] the probability distribution $p(v,t)$ of v is governed by the Fokker–Planck Equation (FPE)

$$\frac{\partial}{\partial t}p(v,t) = \frac{\partial}{\partial v}[R(v)(v - V_e)p] + D\frac{\partial^2}{\partial v^2}p \tag{A.2}$$

Provided a normalizable stationary solution to the above equation exists, it is given by

$$p^{(s)}(v) = N \exp\left\{-\frac{1}{D}\int_{-\infty}^{v} \mathrm{d}\tilde{v}\, R(\tilde{v})(\tilde{v} - V_e)\right\} \tag{A.3}$$

where N is the normalization constant such that the integral of $p^{(s)}(v)$ over v is unity. The stationary distribution in eq A.3 is completely specified by D and the functional form of $R(v)$. The stationary distribution is Gaussian only when $R(v)$ is a constant. In the case when $R(v)$ is not a constant (e.g., when $R(v)$ rapidly decreases when v approaches the hard core volume), a FPE with a constant diffusion coefficient might not even have a stationary solution. The FPE given in eq A.2 is inappropriate for the current situation where $R(v)$ is a strong function of v and the stationary distribution is still required to be Gaussian (i.e., eq 7).

In order to incorporate the strong dependence in $R(v)$, one must start from a general form of FPE given in eq 11 without any *a priori* assumption about the functional form of the diffusive term $B^2(v)$. For a stationary distribution the time derivative in eq 11 is zero. After integrating and rearranging terms, the defining equation for the stationary distribution $p^{(s)}(v)$ is given by

$$A(v)p^{(s)}(v) = \frac{\mathrm{d}}{\mathrm{d}v}\left(\frac{\sigma_e^2}{2}B^2(v)p^{(s)}(v)\right) \tag{A.4}$$

where the constant of integration was set to zero in order to satisfy the boundary conditions that the distribution density and its derivative vanish when v goes to $\pm\infty$. Integrating eq A.4 over the entire domain and employing the boundary conditions once again, we conclude that the $A(v)$ term in the generalized FPE eq 11 must always satisfy the condition

$$\int_{-\infty}^{\infty} \mathrm{d}\tilde{v}\, A(\tilde{v})p^{(s)}(\tilde{v}) = 0 \tag{A.5}$$

Provided the necessary integrals exist, the generalized diffusion coefficient $\sigma_e^2B^2(v)$ can be expressed in terms of $A(v)$ and the stationary distribution as

$$\sigma_e^2B^2(v) = \frac{2}{p^{(s)}(v)}\int_{-\infty}^{v} \mathrm{d}\tilde{v}\, A(\tilde{v})p^{(s)}(\tilde{v}) \tag{A.6}$$

Now if the rate function $R(v)$ in the original deterministic equation is such that

$$\int_{-\infty}^{\infty} \mathrm{d}\tilde{v}\, R(\tilde{v})(\tilde{v} - V_e)p^{(s)}(\tilde{v}) = 0 \tag{A.7}$$

then one simply sets $A(v)$ equal to $-R(v)(v - V_e)$ and the condition (A.5) is satisfied.

A complication arises in the case of a rate function for which eq A.7 does not hold, for example when $R(v)$ is not symmetric with respect to $v = V_e$. In this case we postulate that a new term, which was not present in the original deterministic equation, must be added to the drift part of the stochastic equation $A(v)$ to ensure that the condition of eq A.5 is fulfilled. Having a purely stochastic nature, this term should vanish in the limit of $\sigma_e \to 0$. In the rest of this Appendix we present an argument on how to construct such a term. It should be emphasized, however, that this is by no means a formal derivation.

As follows from the previous discussion, an additional term must cancel out the contribution from the original $-R(v)(v - V_e)$ term when integrated with the stationary distribution $p^{(s)}(v)$. One possibility is to simply subtract the value of the integral from the original term, which gives rise to the following expression (corresponding to case II in the main text)

$$A^{(II)} = -R(v)(v - V_e) + \int_{-\infty}^{\infty} \mathrm{d}\tilde{v}\, R(\tilde{v})(\tilde{v} - V_e)p^{(s)}(\tilde{v}) \tag{A.8}$$

The condition (A.5) is obviously satisfied. The correct deterministic limit is also assured since the integral in eq A.8 vanishes as the stationary distribution $p^{(s)}(v)$ becomes delta function $\delta(v - V_e)$ at $\sigma_e \to 0$. Integrating by parts and noticing that

$$\left\langle \frac{\mathrm{d}R}{\mathrm{d}v} \right\rangle_e = \int_{-\infty}^{\infty} \mathrm{d}\tilde{v}\, \frac{\mathrm{d}R(\tilde{v})}{\mathrm{d}\tilde{v}}p^{(s)}(\tilde{v}) \tag{A.9}$$

Equation A.8 can be converted into the form shown in the main text as eq 10a. Using eq A.6, the magnitude of the fluctuations $B^2(v)$ given in eq 10b is obtained.

dx.doi.org/10.1021/ma300441a | Macromolecules 2012, 45, 7237–7259

However, the solution given in eq A.8 is not unique, since it is possible to construct an infinite number of expressions whose integrals with the $p^{(s)}(v)$ satisfy eq A.5. An example of such an expression would be

$$\tilde{A} = -R(v)(v - V_e) + \frac{1}{3}\left[R(v)\frac{(v - V_e)^3}{\sigma_e^2} - \sigma_e^4\frac{d^3}{dv^3}R(v)\right] \tag{A.10}$$

The recipe for obtaining this and similar formulas is to integrate by parts the products of the stationary distribution and the derivatives of the rate function $R(v)$ of the form

$$p^{(s)}(v)\sigma_e^{n+1}\frac{d^n}{dv^n}R(v) \tag{A.11}$$

However, an inspection shows that all the expressions of this type, except one, contain negative powers of σ_e (e.g., first term in square brackets in eq A.10) and, thus, do not possess the correct deterministic limit. The only expression with the correct deterministic limit as $\sigma_e \to 0$ is (see eq 9a)

$$A^{(I)} = -R(v)(v - V_e) + \sigma_e^2\frac{d}{dv}R(v) \tag{A.12}$$

The magnitude of the fluctuations is determined via integration of $A^{(I)}$ as defined in eq A.6, resulting in the simple expression given in the main text as eq 9b.

Thus, both sets of the drift and diffusive terms denoted as case I and case II in the main text satisfy the stationarity conditions imposed by eq A.5 and have correct macroscopic limit. However, the *dynamic* behaviors described by case I versus case II can be dramatically different, especially for highly asymmetric rate function $R(v)$ as illustrated by inability of the case II based equations to predict Kovacs data.

It is worth noting that the multiple forms of the generalized FPE only appear in the nonlinear case when the rate is a function of the relaxing variable. When $R(v)$ equals a constant, both the integral in eq A.8 and the derivative in eq A.12 are zero. However, this is only true for a one-dimensional system, i.e., one stochastic variable. In case of higher dimensions even a linear deterministic system has an infinite number of stochastic generalizations, each leading to the same stationary distribution. The analysis of a multidimensional system will be described in a subsequent paper.

APPENDIX B. CONNECTION BETWEEN FOKKER–PLANCK AND MASTER EQUATION FORMULATIONS OF THE STOCHASTIC MODEL

The Fokker–Planck equation (FPE) given in eq 11 can be cast into a discrete master equation (ME) form that is more convenient for numerical solution, and the development of the ME form is the objective of this Appendix. The discretized probability distribution $\{p_i\}$ evolves according to a birth–death master equation of the form given by eq 12. The FPE is equivalent to birth–death ME as the discretization step h goes to zero if the downward and upward rates are defined according to eqs 14 (see ref 50 for formal proof). The detailed balance eq 15 puts constraints on the rates $\{k_i^+\}$ and $\{k_i^-\}$ by requiring that stationary distributions have a prescribed form similarly to how in the continuous case eq A.4 puts constraints on the form of the drift term and the diffusive term. Substitution of eq 14 into eq 12 results in the following equation:

$$p_i^{(s)}A_i + p_{i-1}^{(s)}A_{i-1} = \frac{\sigma_e^2}{h}(p_i^{(s)}B_i^2 - p_{i-1}^{(s)}B_{i-1}^2) \tag{B.1}$$

In the limit of $h \to 0$ the discrete eq B.1 becomes eq A.4. Summation over index i from 1 to n in eq B.1 and use of eq 13 leads to

$$\sum_{i=1}^{n} p_i^{(s)}A_i = 0 \tag{B.2}$$

Equation B.2 is a discrete analogue of eq A.5 and represents a condition on the admissible sets of $\{A_i\}$. For a given set of $\{A_i\}$ satisfying eq B.2 the corresponding $\{B_i^2\}$ are calculated according to

$$p_i^{(s)}\sigma_e^2 B_i^2 = 2h\sum_{j=1}^{i-1} p_j^{(s)}A_j + hp_i^{(s)}A_i \tag{B.3}$$

That eq B.3 gives a correct solution can be verified by substitution into eq B.1, where eq B.3 is a discrete analogue of eq A.6.

As in the continuous case the condition (B.2) does not determine the set $\{A_i\}$ uniquely. For instance, a set of n quantities defined according to

$$A_i = F_i - \sum_{j=1}^{n} p_j^{(s)}F_j \tag{B.4}$$

where $\{F_i\}$ are arbitrary, will always satisfy eq B.2. Now if a set $\{F_i\}$ can be found that results in non-negative upward and downward rates $\{k_i^+\}$ and $\{k_i^-\}$, then such a set constitute an admissible ME formulation with the required stationary solution. Use of eqs 14, B.3, and B.4 gives rise to the equations ($i = 2, ..., n$)

$$k_i^- = \frac{1}{hp_i^{(s)}}\left[\sum_{j=1}^{i-1} p_j^{(s)}F_j - \sum_{j=1}^{i-1} p_j^{(s)}\langle F\rangle_e\right] \tag{B.5a}$$

$$k_i^+ = \frac{1}{hp_i^{(s)}}\left[\sum_{j=1}^{i} p_j^{(s)}F_j - \sum_{j=1}^{i} p_j^{(s)}\langle F\rangle_e\right] \tag{B.5b}$$

with $\langle F\rangle_e = \sum_{k=1}^{n} p_k^{(s)}F_k$. Consistent with the continuous case (case II) as well as the deterministic limit, one choice for $\{F_i\}$ is $F_i = -R(v_i)(v_i - V_e)$. Numerical evaluation shows that in this case the rates defined in eqs B.5 are non-negative as required by the definition of $\{k_i^+\}$ and $\{k_i^-\}$, although we have been unable to obtain a formal proof. The ME formulation resulting from this choice of functions $\{F_i\}$, although being mathematically correct, suffers from the disadvantage that the rates are given by complicated expressions B.5 and are difficult to assign an intuitive meaning.

A different class of functions $\{A_i\}$ satisfying eq B.2 is defined as

$$A_i = \frac{\sigma_e^2}{h}\left(R(v_{i+1})\frac{p_{i+1}^{(s)}}{p_i^{(s)}} - R(v_i)\right) \tag{B.6}$$

The condition of eq B.2 will hold for any non-negative set of $\{R(v_i)\}$ with the only requirement that $R(v_1) = 0$. Substituting eq B.6 into eq B.3, one finds

dx.doi.org/10.1021/ma300441a | Macromolecules 2012, 45, 7237–7259

$$B_i^2 = R(v_{i+1})\frac{p_{i+1}^{(s)}}{p_i^{(s)}} + R(v_i) \tag{B.7}$$

Finally, using eqs 14, B.6, and B.7

$$k_i^- = \frac{\sigma_e^2}{h^2}R(v_i) \quad k_i^+ = \frac{\sigma_e^2}{h^2}R(v_{i+1})\frac{p_{i+1}^{(s)}}{p_i^{(s)}} \tag{B.8}$$

Unlike the expressions given in eqs B.5, the formulas (B.8) have a clear physical meaning where $R(v_i)$ plays the role of a local rate of relaxation for a system in the ith state. If one started with an ME formulation without ever considering a corresponding FPE, eqs B.8 would have been a very natural way of defining downward and upward rates $\{k_i^+\}$ and $\{k_i^-\}$ via $R(v_i)$. Equations B.8 (without the σ_e^2 factors) were postulated in the Robertson et al.[20] paper. In order to make the connection between the continuous case given in eqs 9 (case I) and the discrete form given in eqs B.8 more apparent, it is instructive to examine the limit of $h \to 0$. Taking advantage of the expansion $p_{i+1}^{(s)} \approx p_i^{(s)}((1 - (v_i - V_e)/(\sigma_e^2)h)$, one establishes that eqs B.8 are the discrete analogue of case I of the continuous FPE model.

APPENDIX C. METHOD FOR SOLVING THE MASTER EQUATION

The solution of the ME is obtained using standard eigenvector methods. Using a similar approach to that employed by Robertson et al.,[20] the ME (eq 11) for the discretized probability density vector $\mathbf{p}(t) = \{p_i(t)\}$ is expressed in matrix form as

$$\frac{\mathrm{d}}{\mathrm{d}t}\mathbf{p}(t) = \mathbf{K}\cdot\mathbf{p}(t) \tag{C.1}$$

where the nonzero matrix elements of $\mathbf{K}$ are

$$\begin{aligned} K_{i,i-1} &= k_{i-1}^+, \quad i = 2, \ ..., \ n \\ K_{i,i} &= -(k_i^- + k_i^+), \quad i = 1, \ ..., \ n \\ K_{i,i+1} &= k_{i+1}^-, \quad i = 1, \ ..., \ n-1 \end{aligned} \tag{C.2}$$

$\mathbf{K}$ is generally nonsymmetric; however, a similarity transformation can be applied to create a symmetric matrix $\mathbf{Z}$

$$\mathbf{Z} = \mathbf{D}^{-1}\cdot\mathbf{K}\cdot\mathbf{D} \tag{C.3}$$

where $\mathbf{D}$ is a diagonal matrix with the elements $D_{i,i} = D_i$ with the requirement that

$$Z_{i,i-1} = K_{i,i-1}D_{i-1}/D_i = K_{i-1,i}D_i/D_{i-1} = Z_{i-1,i} \tag{C.4}$$

and hence

$$(D_{i-1}/D_i)^2 = K_{i-1,i}/K_{i,i-1} = k_i^-/k_{i-1}^+ \tag{C.5}$$

Invoking the detailed balance equation given in eq 15, it is convenient to define the matrix elements of $\mathbf{D}$ as

$$D_i = \sqrt{p_i^{(s)}} \tag{C.6}$$

Thus, the final expression for the matrix elements of $\mathbf{Z}$ in terms of the equilibrium distribution $\{p_i^{(s)}\}$ of the specific volume and the transition rates reads

$$\begin{aligned} Z_{i,i} &= -(k_i^- + k_i^+), \quad i = 1, \ ..., \ n \\ Z_{i,i+1} &= k_{i+1}^-\sqrt{p_{i+1}^{(s)}/p_i^{(s)}}, \quad i = 1, \ ..., \ n-1 \end{aligned} \tag{C.7}$$

The ME given in eq C.1 now becomes

$$\frac{\mathrm{d}}{\mathrm{d}t}[\mathbf{D}^{-1}\cdot\mathbf{p}(t)] = \mathbf{Z}\cdot[\mathbf{D}^{-1}\cdot\mathbf{p}(t)] \tag{C.8}$$

with the solution

$$\mathbf{p}(t) = \mathbf{D}\cdot\mathbf{Q}\cdot\exp[t\mathbf{\Lambda}]\cdot\mathbf{Q}^{-1}\cdot\mathbf{D}^{-1}\cdot\mathbf{p}(0) \tag{C.9}$$

where $\mathbf{Q}$ is the matrix formed from the normalized (column) eigenvectors of $\mathbf{Z}$, and $\mathbf{\Lambda}$ is the diagonal matrix of the eigenvalues of $\mathbf{Z}$. Returning to indexical notation

$$p_i(t) = \sum_{k=1}^{n}\sqrt{p_i^{(s)}}\,Q_{ik}\mathrm{e}^{\lambda_k t}\sum_{j=1}^{n}Q_{jk}\frac{1}{\sqrt{p_j^{(s)}}}p_j(0) \tag{C.10}$$

The largest eigenvalue λ_1, which corresponds to the stationary state, is always zero, and the rest of the eigenvalues are negative. The components of the eigenvector associated with the stationary solution are given by

$$Q_{i1} = \sqrt{p_i^{(s)}}\, i = 1, \ ..., \ n \tag{C.11}$$

The remaining eigenvalues/vectors for the matrix $\mathbf{Z}$ can be determined numerically using standard[87] techniques. However, when the ratio of smallest to largest values of the transition rates k_1^+/k_n^- is less than the machine precision, the numerical solution based upon standard algorithms becomes impossible. A perturbation solution has been developed for these cases as described in the Supporting Information.

The ME requires specification of the level of discretization of the naturally continuous volume distribution. The choice of the discretization step h, and therefore the rank n of the $\mathbf{Z}$ and $\mathbf{Q}$ matrices, is dictated by the desired accuracy in approximating the continuous volume distribution. In addition, the requirement that the transition rates in eqs 14 always be positive puts some constraints on h; specifically

$$h < \min\left(\frac{\sigma_e^2 B^2(v_1)}{A(v_1)}; \ \frac{\sigma_e^2 B^2(v_n)}{|A(v_n)|}\right) \tag{C.12}$$

The requirement on h defined by eq C.12 will become a problem for sufficiently small volumes (i.e., for the smallest volume v_1 accessible to the system) when the diffusive term $\sigma_e^2 B^2(v,T)$ vanishes faster than the drift term $A(v,T)$. The requirements imposed by eq C.12 become more severe as the temperature is lowered because $R(v,T)$ is a steeper function of v at lower T. Of course, h could always be decreased, but then the size of the $\mathbf{Z}$ and $\mathbf{Q}$ matrices becomes computationally infeasible.

Solution Procedure

The solution procedure for the isothermal response of the stochastic model following a small temperature step is as follows:

1. The range of specific volumes available to a meso-domain is discretized, resulting in the $\{v_i\}$ set, taking care to satisfy the constraints given in eq C.12.

2. The downward and upward transition rates $\{k_i^-\}$, $\{k_i^+\}$ are calculated via eqs 14, where the formulas for $A(v_i)$ and $B^2(v_i)$

dx.doi.org/10.1021/ma300441a | Macromolecules 2012, 45, 7237−7259

are given by eqs 9 for case I and by eqs 10 for case II. The log $a(v_i,T)$ function is given in eq 23.

3. The **Z** matrix is calculated via C.7, and its eigenvectors/values are obtained.

4. The specific volume distribution function $\{p_i(t)\}$ is calculated from the solution of the ME using eq C.10.

5. Using the distribution function, any average quantity of interest (e.g., the macroscopic specific volume) is calculated.

Our use of the mean-field approximation requires a clarification as to how the solution algorithm is organized, since the current relaxation rate for a given domain depends both on the current local volume and the current average volume. In fact, the average specific volume $V(t)$ is evaluated after every time step and then used in calculation of the transition rates in the ME for the next step via eq 23.

■ ASSOCIATED CONTENT

Supporting Information

Normalized form of the FPE; detailed comparison to the Robertson et al. model; perturbation technique for solving the ME. This material is available free of charge via the Internet at http://pubs.acs.org.

■ AUTHOR INFORMATION

Corresponding Author

*E-mail caruther@ecn.purdue.edu.

Present Address

[†]DuPont Protection Technologies, Wilmington, DE 19880.

Notes

The authors declare no competing financial interest.

■ ACKNOWLEDGMENTS

This work was supported by the National Science Foundation (Grant NIRT 0506840). The authors thank Ritwik Bhatia for useful discussions.

■ REFERENCES

(1) McKenna, G. B.; Simon, S. L. The glass transition; Its measurement and underlying physics. In *Handbook of Thermal Analysis and Calorimetry*; Cheng, S. Z. D., Ed.; Elsevier: Amsterdam, 2002; Vol. 3, pp 49−109.

(2) Alba-Simionesco, C.; Fan, J.; Angell, C. A. *J. Chem. Phys.* **1999**, *110* (11), 5262−5272.

(3) Greaves, G. N.; Sen, S. *Adv. Phys.* **2007**, *56* (1−2), 1−166.

(4) Guntherodt, H. J.; Beck, H. *Glassy Metals III: Amorphization Techniques, Catalysis, Electronic and Ionic Structure*; Springer: Berlin, 1994.

(5) In 6th International Discussion Meeting on Relaxation in Complex Systems, Rome, 2009. Ngai, K. L.; Ruocco, G., Eds. *J. Non-Cryst. Solids*, **2011**, *357*, (2), 241−782.

(6) Kovacs, A. J. *J. Polym. Sci.* **1958**, *30* (121), 131−147.

(7) Kovacs, A. J. *Fortschr. Hochpolym.-Forsch.* **1963**, *3*, 394−507.

(8) Rychwalski, R. W.; Delin, M.; Kubat, J. *Mech. Time-Depend. Mater.* **1997**, *1*, 161−180.

(9) Uchidoi, M.; Adachi, K.; Ishida, Y. *Polym. J.* **1978**, *10* (2), 161−167.

(10) Greiner, R.; Schwarzl, F. R. *Colloid Polym. Sci.* **1989**, *267* (1), 39−47.

(11) Bernazzani, P.; Simon, S. L. *J. Non-Cryst. Solids* **2002**, *307−310*, 470−480.

(12) Simon, S. L.; Bernazzani, P. *J. Non-Cryst. Solids* **2006**, *352* (42−49), 4763−4768.

(13) Bero, C. A.; Plazek, D. J. *J. Polym. Sci., Part B: Polym. Phys.* **1991**, *29* (1), 39−47.

(14) Schultheisz, C. R.; McKenna, G. B. In *Volume Recovery and Physical Aging in Glassy Polycarbonate Following Temperature Jumps*, NATAS 25th Annual Conference, 1997; pp 366−373.

(15) McKenna, G. B.; Vangel, M. G.; Rukhin, A. L.; Leigh, S. D.; Lotz, B.; Straupe, C. *Polymer* **1999**, *40* (18), 5183−5205.

(16) Geener, J.; O'Reilly, J. M.; Ng, K. C. The Volumetric Response of Polymeric Glasses to Complex Thermomechanical Histories: a Critical Evaluation of the KAHR Model. In *Structure, Relaxation, and Physical Aging of Glassy Polymers*; Roe, R. J., O'Reilly, J. M., Torkelson, J., Eds.; Materials Research Society: Pittsburgh, 1991; Vol. *215*, pp 99−107.

(17) Knauss, W. G.; Emri, I. *Polym. Eng. Sci.* **1987**, *27* (1), 86−100.

(18) Kovacs, A. J.; Aklonis, J. J.; Hutchinson, J. M.; Ramos, A. R. *J. Polym. Sci., Polym. Phys. Ed.* **1979**, *17*, 1097−1162.

(19) Matsuoka, S.; Williams, G.; Johnson, G. E.; Anderson, E. W.; Furukawa, T. *Macromolecules* **1985**, *18* (12), 2652−2663.

(20) Robertson, R. E.; Simha, R.; Curro, J. G. *Macromolecules* **1984**, *17* (4), 911−919.

(21) Vleeshouwers, S.; Nies, E. *Macromolecules* **1992**, *25* (25), 6921−6928.

(22) Vleeshouwers, S.; Nies, E. *Colloid Polym. Sci.* **1996**, *274* (2), 105−111.

(23) Lustig, S. R.; Shay, R. M. J.; Caruthers, J. M. *J. Rheol.* **1996**, *40* (1), 69−106.

(24) Caruthers, J. M.; Adolf, D. B.; Chambers, R. S.; Shrikhande, P. *Polymer* **2004**, *45*, 4577−4597.

(25) Lindsey, C. P.; Patterson, G. D. *J. Chem. Phys.* **1980**, *73* (7), 3348−3357.

(26) McKinney, J. E.; Goldstein, M. *J. Res. Natl. Bur. Stand., Sect. A* **1974**, *78A* (3), 331−353.

(27) Ng, D.; Aklonis, J. J. Multiple Ordering Parameter Models of the Glass Transition and Approaches to Equilibrium. In *Relaxation in Complex Systems*; Ngai, K. L., Wright, G. B., Eds.; Naval Research Laboratory: Springfield, VA, 1985; pp 53−63.

(28) Struik, L. C. E. *Polymer* **1997**, *38*, 4677−4685.

(29) Robertson, R. E.; Simha, R.; Curro, J. G. *Macromolecules* **1988**, *21* (11), 3216−3220.

(30) Robertson, R. E. *J. Polym. Sci., Polym. Phys. Ed.* **1979**, *17*, 597−613.

(31) Sillescu, H. *J. Non-Cryst. Solids* **1999**, *243*, 81−108.

(32) Ediger, M. D. *Annu. Rev. Phys. Chem.* **2000**, *51*, 99−128.

(33) Berthier, L.; Biroli, G. *Rev. Mod. Phys.* **2011**, *83* (2), 587−645.

(34) Schmidt-Rohr, K.; Spiess, H. W. *Phys. Rev. Lett.* **1991**, *66* (23), 3020−3023.

(35) Tracht, U.; Wilhelm, M.; Heuer, A.; Feng, H.; Schmidt-Rohr, K.; Spiess, H. W. *Phys. Rev. Lett.* **1998**, *81* (13), 2727−2730.

(36) Tracht, U.; Wilhelm, M.; Heuer, A.; Spiess, H. W. *J. Magn. Reson.* **1999**, *140*, 460−470.

(37) Leisen, J.; Schmidt-Rohr, K.; Spiess, H. W. *J. Non-Cryst. Solids* **1994**, *172*, 737−750.

(38) Li, K. L.; Jones, A. A.; Inglefield, P. T.; English, A. D. *Macromolecules* **1989**, *22* (11), 4198−4204.

(39) Bokov, N. A. *J. Non-Cryst. Solids* **1994**, *177*, 74−80.

(40) Lee, M.; Saha, S. K.; Moynihan, C. T.; Schroeder, J. *J. Non-Cryst. Solids* **1997**, *222*, 369−375.

(41) Moynihan, C. T.; Schroeder, J. *J. Non-Cryst. Solids* **1993**, *160*, 52−59.

(42) Moynihan, C. T.; Schroeder, J. *J. Non-Cryst. Solids* **1993**, *161*, 148−151.

(43) Jeffrey, K. R.; Richert, R.; Duvvari, K. *J. Chem. Phys.* **2003**, *119* (12), 6150−6156.

(44) Wendt, H. *Phys. Rev. E* **2000**, *61* (2), 1722−1728.

(45) Ediger, M. D. *J. Non-Cryst. Solids* **1998**, *235*, 10−18.

(46) Stillinger, F. H.; Hodgdon, J. A. *Phys. Rev. E* **1994**, *50* (3), 2064−2068.

(47) Russell, E. V.; Israeloff, N. E.; Walther, L. E.; Gomariz, H. A. *Phys. Rev. Lett.* **1998**, *81* (7), 1461−1464.

(48) Russell, E. V.; Israeloff, N. E. *Nature* **2000**, *408* (6813), 695−698.

(49) Donati, C.; Glotzer, S. C.; Poole, P. H.; Kob, W.; Plimpton, S. J. *Phys. Rev. E* **1999**, *60* (3), 3107−3119.
(50) Zhang, W.-B.; Zou, X.-W.; Jin, Z.-Z.; Tian, D.-C. *Phys. Rev. E* **2000**, *61* (3), 2805−2808.
(51) Barrat, J.-L.; Baschnagel, J.; Lyulin, A. *Soft Matter* **2010**, *6* (15), 3430−3446.
(52) Adam, G.; Gibbs, J. H. *J. Chem. Phys.* **1965**, *43* (1), 139−146.
(53) Schapery, R. A. *Polym. Eng. Sci.* **1969**, *9* (4), 295−310.
(54) Gardiner, C. W. *Handbook of Stochastic Methods*; Springer-Verlag: Berlin, 1985; Vol. *13*, p 442.
(55) Scherer, G. W. *J. Am. Ceram. Soc.* **1984**, *67* (7), 504−511.
(56) Tschoegl, N. W.; Knauss, W. G.; Emri, I. *Mech. Time-Depend. Mater.* **2002**, *6* (1), 53−99.
(57) Narayanaswamy, O. S. *J. Am. Ceram. Soc.* **1971**, *54* (10), 491−498.
(58) O'Reilly, J. M. *J. Polym. Sci.* **1962**, *57*, 429−444.
(59) Mead, D. J.; Fuoss, R. M. *J. Am. Chem. Soc.* **1941**, *63*, 2832−2840.
(60) Heinrich, W.; Stoll, B. *Colloid Polym. Sci.* **1985**, *263* (11), 873−878.
(61) Beiner, M.; Korus, J.; Lockwenz, K.; Schroter, K.; Donth, E. *Macromolecules* **1996**, *29* (15), 5183−5189.
(62) Richert, R. *Physica A* **2000**, *287* (1−2), 26−36.
(63) Bair, H. E.; Johnson, G. E.; Anderson, E. W.; Matsuoka, S. *Polym. Eng. Sci.* **1981**, *21* (14), 930.
(64) Joseph, S. H.; Duckett, R. A. *Polymer* **1978**, *19*, 844−849.
(65) Kovacs, A. J.; Stratton, R. A.; Ferry, J. D. *J. Phys. Chem.* **1963**, *67*, 152−161.
(66) Parry, E. J.; Tabor, D. *Polymer* **1973**, *14*, 628−631.
(67) Williams, M. L.; Ferry, J. D. *J. Colloid Sci.* **1954**, *9*, 479−492.
(68) Ninomiya, K.; Fujita, H. *J. Colloid Sci.* **1957**, *12*, 204−229.
(69) Ninomiya, K.; Ferry, J. D. *J. Phys. Chem.* **1963**, *67*, 2292−2296.
(70) Fujino, K.; Horino, T.; Miyamoto, K.; Kawai, H. *J. Colloid Sci.* **1961**, *16*, 411−430.
(71) Schmieder, K.; Wolf, K. *Kolloid Z. Z. Polym.* **1953**, *134* (2−3), 149−185.
(72) Sandberg, O.; Backstrom, G. *J. Polym. Sci., Polym. Phys. Ed.* **1980**, *18*, 2123−2133.
(73) Sasabe, H.; Moynihan, C. T. *J. Polym. Sci., Polym. Phys. Ed.* **1978**, *16*, 1447−1457.
(74) Ferry, J. D. *Viscoelsctic Properties of Polymers*, 3rd ed.; John Wiley & Sons: New York, 1980; p 641.
(75) Plazek, D. J. *Polym. J.* **1980**, *12* (1), 43−53.
(76) Hopkins, I. L. *J. Polym. Sci.* **1958**, *28* (118), 631−633.
(77) Moreland, L. W.; Lee, E. H. *Trans. Soc. Rheol.* **1960**, *4*, 233−263.
(78) Plazek, D. J. *J. Phys. Chem.* **1965**, *69*, 3480−3487.
(79) Arbe, A.; Colmenero, J.; Monkenbusch, M.; Richter, D. *Phys. Rev. Lett.* **1998**, *81* (3), 590−593.
(80) Plazek, D. J.; Plazek, D. L. *Macromolecules* **1983**, *16* (9), 1469−1475.
(81) Truesdell, C.; Noll, W. *The Non-Linear Field Theories of Mechanics*; Springer-Verlag: Berlin, 1965; Vol. *III*, p 602.
(82) Coleman, B. D. *Arch. Ration. Mech. Anal.* **1964**, *17*, 1−46.
(83) Lee, H.-N.; Paeng, K.; Swallen, S. F.; Ediger, M. D. *Science* **2009**, *323*, 231−234.
(84) Frank, T. D. *Physica A* **2001**, *301*, 52−62.
(85) Yoshimoto, K.; Jain, T. S.; Van Workum, K.; Nealey, P. F.; de Pablo, J. J. *Phys. Rev. Lett.* **2004**, *93*, 175501.
(86) MacNeil, D.; Rottler, J. *Phys. Rev. E* **2010**, *81*, 011804.
(87) Press, W. H.; Teukolsky, S. A.; Vetterling, W. T.; Flannery, B. P. *Numerical Recipes in C++*; Cambridge University Press: Cambridge, 2002; p 1003.